Graphical Abstract

Non-linear response of a swirl-stabilized flame to high frequency transverse acoustic excitation

Ravi Gupta, Pratikash P. Panda

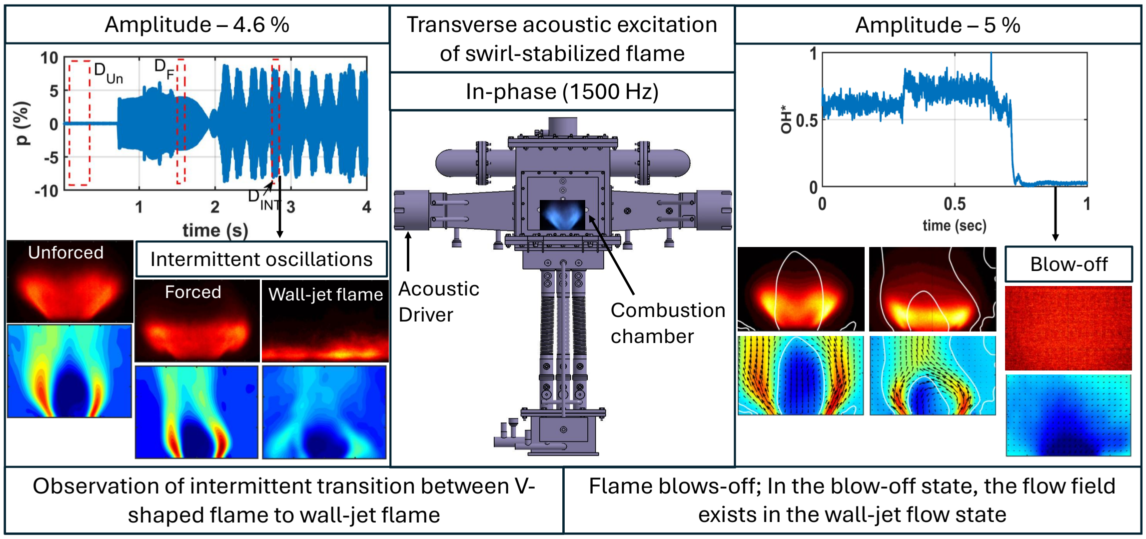

Highlights

Non-linear response of a swirl-stabilized flame to high frequency transverse acoustic excitation

Ravi Gupta, Pratikash P. Panda

- Experimental investigation of a swirl-stabilized partially-premixed flame subjected to high-frequency transverse acoustic forcing at 1500 Hz.
- Identification of non-linear flame response and transition from periodic behavior to Type-II intermittency with increasing acoustic forcing amplitude.
- Phase space reconstruction and recurrence analysis reveal onset of chaotic dynamics and precursors to flame blow-off.
- Flow-field measurements demonstrate transition from columnar vortex breakdown to wall-jet flow structure under strong transverse excitation.
- Dynamical blow-off mechanism linked to flow and flame transition to a wall jet state and possibly due to enhanced heat loss in wall-jet flame configuration.
- Findings provide critical insights into non-linear flame-acoustic coupling, informing stability control strategies for gas turbine combustors.

Non-linear response of a swirl-stabilized flame to high frequency transverse acoustic excitation

Ravi Gupta[a], Pratikash P. Panda[a]

[a]*Department of Aerospace Engineering, Indian Institute of Science, Bangalore, CV Raman Road, Bangalore, 560012, Karnataka, India*

Abstract

The non-linear response of a swirl-stabilized, partially-premixed flame subjected to high-frequency transverse acoustic excitation is experimentally investigated. Motivated by azimuthal thermo-acoustic instabilities in gas turbine combustors, experiments are conducted in a model gas turbine combustor using simultaneous high-speed particle image velocimetry (PIV), OH* chemiluminescence, and unsteady pressure measurements. The flame is excited at 1500 Hz with varying forcing amplitudes, corresponding to 1.6–5.0% of chamber pressure. At low forcing amplitudes, the flame maintains a periodic V-shaped structure with stable, linear acoustic-flame coupling. Increasing the forcing amplitude induces amplitude modulations and spectral broadening, signaling the onset of non-linear interactions. Phase space reconstructions and recurrence analyses reveal a transition to Type-II intermittency, characterized by bursts of high-amplitude oscillations interspersed with low-amplitude states. At higher amplitudes, strong intermittency and chaotic behavior are observed, leading to flame blow-off. The flame dynamics are closely linked to transitions in the underlying flow structure, with the swirling jet evolving from a columnar vortex breakdown (V-flame) to a wall-jet (wall-flame) configuration under strong transverse excitation. This transition promotes heat loss to the combustor walls and destabilizes the flame. Cross wavelet transform analysis highlights a progressive loss of phase-locking between pressure and heat release rate fluctuations with increasing forcing amplitude. The results emphasize the critical role of non-linear flame dynamics and flow-flame-acoustic coupling in driving combustion instabilities under high-frequency excitation. This study provides new insights into the mechanisms governing intermittent behavior and blow-off in swirl-stabilized flames, with implications for the design of more robust, low-emission com-

bustion systems.

Keywords:
Swirl-stabilized flame, transverse acoustic forcing, high frequency instability, wall-jet flame.

(i) Novelty and Significance Statement

This work provides a novel experimental investigation of the non-linear response of a swirl-stabilized, partially-premixed flame to high-frequency transverse acoustic forcing, a configuration that closely mimics azimuthal instabilities in annular combustors. The work systematically explores the effect of large amplitude, high-frequency transverse perturbations, revealing a transition from linear periodic behavior to complex Type-II intermittency and chaotic flame dynamics which is not reported elsewhere. Using a combination of high-speed PIV, OH* chemiluminescence, pressure measurements, phase-space reconstruction, recurrence quantification, and cross wavelet analysis, the study demonstrates that flame blow-off is closely linked to a fundamental flow-field transition from a vortex breakdown-dominated columnar jet to a wall-jet configuration. The results establish a critical connection between acoustic forcing, base flow modification, and intermittent flame behavior, offering valuable insights for the design and stability control of modern low-emission combustion systems operating under challenging high-frequency conditions.

1. Introduction

Gas turbine combustors face a major challenge of obtaining a stable combustion process throughout their operation. The operating conditions of high flow Reynolds number (*Re*) inside these engines make combustion a highly transient process. Thermo-acoustic instabilities, arising from complex interactions between unsteady heat release and acoustic pressure fluctuations, pose a critical challenge in the design and operation of modern combustion systems. These instabilities often emerge in low-emission combustion technology used in aerospace propulsion and power generation as a result of their sensitivity to turbulent fluctuations (1; 2; 3; 4; 5). The instability leads to large-amplitude pressure and velocity oscillations, which result in thrust oscillations, severe vibrations that interfere with control-system, enhanced heat transfer and thermal stresses to combustor walls, oscillatory mechanical loads that result in low- or high-cycle fatigue of system components, and flame blow-out or flashback (6).

In aviation gas turbines, large circumferential length of annular combustor compared to the streamwise length and the annular distribution of multiple injectors (with possibility of flow/flame interaction of adjacent injectors) in the combustion chamber makes azimuthal thermo-acoustic modes relevant for investigation (6; 7). Worth and Dawson (8) have reported observation of circumferential spinning mode due to self-excited instability in an annular combustor with variation in spacing between the injectors. It is observed that as the spacing between the injectors is reduced (from 2.33D to 1.87D to 1.56D), due to interaction of flame of adjacent injectors a circumferential mode is established in the combustor. With the development of self-excited azimuthal mode, it was observed that the pressure fluctuations inside the combustor varied from 2% to $< 6\%$ of mean chamber pressure for a range of equivalence ratio > 0.8 and < 1.0. Alhaffar et al. (9) reported comparison of flame dynamics in an annular combustor (MICCA-Spray) operating under self-sustained azimuthal thermo-acoustic oscillations with those in a linear combustor (TACC-Spray) subjected to external transverse acoustic forcing. By measuring pressure-based flame describing functions (FDFs) across a range of pressure oscillation amplitudes and at different flame positions relative to the acoustic field (pressure, intensity, and velocity anti-nodes), the authors demonstrate a strong similarity between the forced and self-sustained conditions in terms of FDF gain and phase behavior. These findings validate the use of a linear array, externally forced experimental system to reliable reproduce azimuthal instability conditions in annular combustors. Multiple groups have investigated the response of flame to transverse acoustic excitation which in a way mimics the self-excited circumferential instability developed inside an annular combustor. It is reported that a flame located at a pressure anti-node location shows axial oscillations, while the flame at the pressure node shows lateral oscillations (10; 11; 12; 13; 14; 15; 16; 17; 18; 19).

Recent high-fidelity experiments have revealed that combustors, especially multi-injector annular systems, frequently operate in an intermittent regime—characterized by random bursts of high-amplitude oscillations alternating with low-amplitude states. A number of mechanisms are attributed to the non-linear response of the flame (that leads to finite-amplitude limit cycle oscillations) such as changes in the flame surface area (20; 21), fluctuations in local equivalence ratio which alters the flame speed (22; 3), fluctuations in flame speed (23), local/global flame extinction (24; 25), and saturation in the heat release rate (25). Traditional linear theories provide a first approximation of instability onset, but they fall short in capturing the full spectrum of non-linear behaviors, such as complex transitions, non-linear oscillations, and flame extinction events observed in practical systems. Recent studies have revealed that many combustors do not transition smoothly into instability. Instead, they often exhibit intermittent dynamics, where bursts of periodic oscillations are interspersed with quiescent or chaotic phases. Kabiraj and Sujith (26) demonstrated that this intermittency, particularly Type II, precedes flame blowout in laminar flames and arises from non-linear bifurcations. Furthermore, the authors emphasize that many combustion systems, especially those operating close to lean blow-out, exhibit a rich array of non-linear dynamical phenomena including limit cycles, quasi-periodicity, chaos, and intermittency, which cannot be understood without the tools of non-linear dynamical systems theory. The study identifies a subcritical Hopf bifurcation that triggers the transition from a non-oscillatory regime to a self-excited limit cycle oscillation. As the flame location is further changed, the system progresses through a secondary Hopf bifurcation to quasi-periodic oscillations, and eventually to an intermittent regime marked by bursts of high-amplitude oscillations interspersed with chaotic laminar phases. The authors demonstrate that this final intermittent state (Type II) precedes flame blowout, making it a critical phase to understand for instability prediction and control. Mariappan and Mohan (27) examined a multi-burner annular combustor and identified that flame transient phenomena—including local extinction and re-ignition events—modulate acoustic modes, leading to stochastic self-excited pressure bursts. These dynamics are best captured by non-linear low-order models incorporating stochastic components and experimentally derived transient time scales. Complementing these findings, Durox et al. (28) have reported that self-excited circumferential instability in an annular combustor can have different effects such as a low frequency switch in the flame shape. Auzillon et al. (29) investigated swirling spray flames subjected to transverse acoustic forcing and observed dynamic blowout events. Their work highlights that deterministic acoustic perturbations can induce complex flame behaviors, validating the role of both external forcing and internal flame dynamics in destabilizing combustion. Together, these studies emphasize the need to move beyond classical linear frameworks and adopt non-linear dynamical systems approaches for better prediction and control of combustion instabilities.

Recent studies have highlighted the increased risk of inducing high-frequency self-excited thermo-acoustic instabilities in hydrogen enriched combustors (30), (31), (32). Paniez et al.(32) reported a self-excited, high-frequency thermo-acoustic instability occurring at approximately 4893 Hz in a partially premixed dual-swirled hydrogen burner. The authors explore a unique case where transverse acoustic modes are excited in the absence of significant injector or axial acoustic coupling. Using pressure measurements, OH^* chemiluminescence, and PIV/OH-PLIF diagnostics, the instability is attributed to a rotating transverse mode synchronized with helical vortex structures generated in the flame shear layers. These structures, in phase with the transverse acoustic field, reinforce the oscillations and generate a spinning acoustic mode aligned with the flame swirl direction. A low-order model incorporating transverse acoustics and a simplified V-shaped flame geometry successfully predicts the onset of instability through a positive Rayleigh index, which increases with flame area and hydrogen velocity. Ahn et al. (31) report the dynamic flame response to azimuthal thermoacoustic instabilities in a pressurized annular combustor operating with methane-hydrogen mixtures. The work highlights the potential for hydrogen enriched fuel to introduce high-frequency and harmonic pressure oscillations that may influence combustor stability. Using high-speed OH^* chemiluminescence and pressure measurements, the study demonstrates that although higher-order harmonics are present in the pressure field, the global heat release rate (HRR) is dominated by the fundamental azimuthal mode. The HRR response shows a near-linear scaling with velocity oscillations and exhibits increasing phase lag with higher hydrogen content, consistent with the Rayleigh criterion. Interestingly, while high-frequency acoustic components are present, their spatial phase distribution leads to partial cancellation in the global HRR, reducing their impact on driving instabilities. These findings underscore the importance of considering both frequency content and spatial structure when evaluating the role of high-frequency thermo-acoustic interactions in annular combustors fueled with hydrogen-rich mixtures.

The primary objective of this work is to investigate the response of a swirl stabilized partially premixed flame to high frequency transverse acoustic excitation. The work particularly focuses on the effect of large amplitude pressure oscillations leading to non-linear effects in a swirl-stabilized flame. The study includes experimental investigation of the response of a swirl-stabilzed flame using simultaneous two-dimensional two-component (2D-2C) particle image velocimetry (PIV), line-of-sight integrated OH* chemiluminescence and unsteady pressure measurement. The paper is structured as follows: Section 2 provides the details of the experimental test setup, diagnostic techniques used for experiments and the experimental test conditions. Section 3 presents the results and discussions. Section 4 provides a summary and final conclusion of this work.

2. Methodology

2.1. Details of the experimental test setup

A multi-nozzle linear array combustion chamber is designed and fabricated to study single/multiple interacting swirling jets/flames. Since our motivation for the present study stems from the azimuthal (or transverse) instabilities in annular gas turbine combustors, the current experimental setup is designed to understand the response of non-reacting and reacting swirling flows to external transverse acoustic excitation. Therefore, the test apparatus features external acoustic excitation on a swirl-stabilized jet (or flame) in the direction transverse to the flow. Figure 1 shows the front and side view of the experimental test apparatus. The test apparatus consists of a combustion chamber, flow feed lines, settling chamber, acoustic drivers, ducts connecting the acoustic drivers to the combustion chamber, and exhaust duct. The combustion chamber has a cuboidal geometry with a height of $12D$ in the streamwise direction (x), width of $11.3D$ in the transverse direction (along the acoustic drivers) (r), and depth of $5D$. Here, D (23.36 mm) represents the diameter of the injector at the combustor dump plane. In this work, D is used as a characteristic dimension to compute flow Reynolds number (Re), and to normalize any spatial dimension. The cuboidal arrangement represents an unwrapped geometry of a sector of an annular gas turbine combustor, where the design is such that we can investigate the interaction of up to three swirl injectors. The straight walls do not mimic the effect of curvature in an annular combustor; however, they allow ease of optical diagnostics. The injector is $2.5D$ away from the walls, ensuring minimum influence of the combustor walls on the flow dynamics.

The flow enters the combustion chamber by passing through a flush mounted swirl injector placed upstream of the combustor dump plane. The injector is mounted on a separate injector block which is black-anodized on the surface facing the combustor to minimize laser reflection. Upstream to the injector, the test apparatus consists of a settling chamber. The settling chamber has a series of honeycomb mesh to ensure a uniform flow to pass through it. The air enters the settling chamber from a pressurized reservoir and the flow rate into the settling chamber is controlled and measured using a mass-flow-controller (MFC, make: Alicat Scientific). The flow enters from the settling chamber to feed line connecting the combustor chamber. The flow in the feed line passes through an orifice plate to provide an acoustically closed boundary condition. Static pressure sensors are mounted upstream and downstream to the orifice. This allows determining the mass flow rate through each individual feed line. The mass flow rate through the orifice plate is calculated by measuring static pressure upstream and downstream of the orifice plate. The orifice plate is calibrated by allowing a known mass flow rate of air to pass through the feed line and measuring the pressure upstream and downstream of the orifice plate. The combustor exhaust gases exits through exhaust ducts placed on the two lateral sides of the combustion chamber (CC). The placement of exhaust ducts allows for complete optical access to the CC through the top. This is required because the acoustic excitations are provided from the sides which mandate the laser sheet to enter through the top. A pair of acoustic waveguides of length 276 mm are placed on the two lateral sides of the CC. A set of two acoustic drivers (details are provided in the subsequent section) are connected to each of the acoustic waveguides that perturb the flame inside the CC in the transverse direction. The experimental test rig is made of stainless steel (SS-316L) including the combustion chamber, inlet duct, settling chamber, and acoustic waveguides. The injector is manufactured using additive manufacturing technique with precipitation-hardened stainless steel (17-4 PH). An additional block - fuel block, is placed upstream to the injector block to allow the fuel supply to the fuel nozzle (the centerbody of the injector acts as a fuel nozzle). The details of the injector and the fuel nozzle is provided in subsequent sections. An axial swirl injector (with axial vanes) is used to provide the swirl motion to the incoming air flow. The injector is placed upstream and flush-mounted to the combustor dump plane. The injector consists of 8 clockwise-oriented straight uniformly thick (1.74 mm) axial vanes (vane angle (θ) $= 55^o$ with the axis of the injector), a cylindrical center body, a convergent-divergent passage, and a flare at a diverging angle of 35^o. Figure 2 shows the sectional view of the injector assembly. The direction of the flow is from bottom towards the top (w.r.t to the front view). The convergent-divergent section is typical of the lean-direct injection (LDI) injector where the convergent section ensures higher oxidizer velocity to prevent flashback, and the divergent part ensures the greater spread of fuel injected through the center body (acting as fuel nozzle). The convergent and divergent sections have an angle of 40.8^o and

35^o, respectively. The centerbody which also acts as a fuel nozzle is cylindrical with diameter 6.5 mm and terminates 6.5 mm upstream to the dump plane. The fuel nozzle consists of 8 uniformly spaced circular holes (diameter = 0.7 mm) in the azimuthal direction. Fuel is injected radially outward into the converging section of the injector, 12.5 mm upstream to the combustor dump plane as shown in the figure 2. The exit diameter of the injector at the dump plane is 23.36 mm. This diameter is used as the characteristic length scale while calculating the flow Reynolds number (Re) through the injector. The geometric swirl number (SN_G) is calculated using Eq. (1) provided in Gupta et al., (33). For current swirler geometry, $d = 24$ mm, $d_h = 9$ mm and $\theta = 55°$. The geometric swirl number of the swirler is calculated as 1.049. The injector dimensions used in the formulation - d and d_h are shown in the figure 2.

$$SN = \frac{2}{3}\left[\frac{(1-(d_h/d)^3)}{(1-(d_h/d)^2}\right] tan\theta \tag{1}$$

where, θ is the vane angle,
d_h is the inner hub diameter (shown in the figure 2),
d is the outer hub diameter (shown in the figure 2).

During all future discussions, we assume that the geometric center of the injector at the dump plane as the origin, and x, r, θ represent the streamwise, transverse (or radial), and azimuthal directions, respectively.

Optical access to the inside of the combustion chamber (CC) is provided using quartz windows placed at the front and top of the chamber. The laser sheet enters through the top window and the visualization is performed through the front window in the streamwise mid-plane ($x - r$).

2.2. Acoustic Forcing

A pair of $400W$ BMS 4599ND acoustic drivers are used for acoustic excitation. The two acoustic drivers are placed on each side of the combustion chamber in the transverse direction. These are connected to the combustion chamber with the help of ducts (shown in the figure 1). A range of acoustic conditions, such as standing wave or traveling wave, can be realized by operating the two acoustic drivers at different frequencies and amplitudes, and triggering them in-phase or out-of-phase. Operating the two acoustic drivers with equal excitation amplitude in in-phase (IP) and out-of-phase (OP) condition establishes a pressure antinode (or velocity node) and pressure node (or velocity antinode) at the center of the combustor, respectively. A two

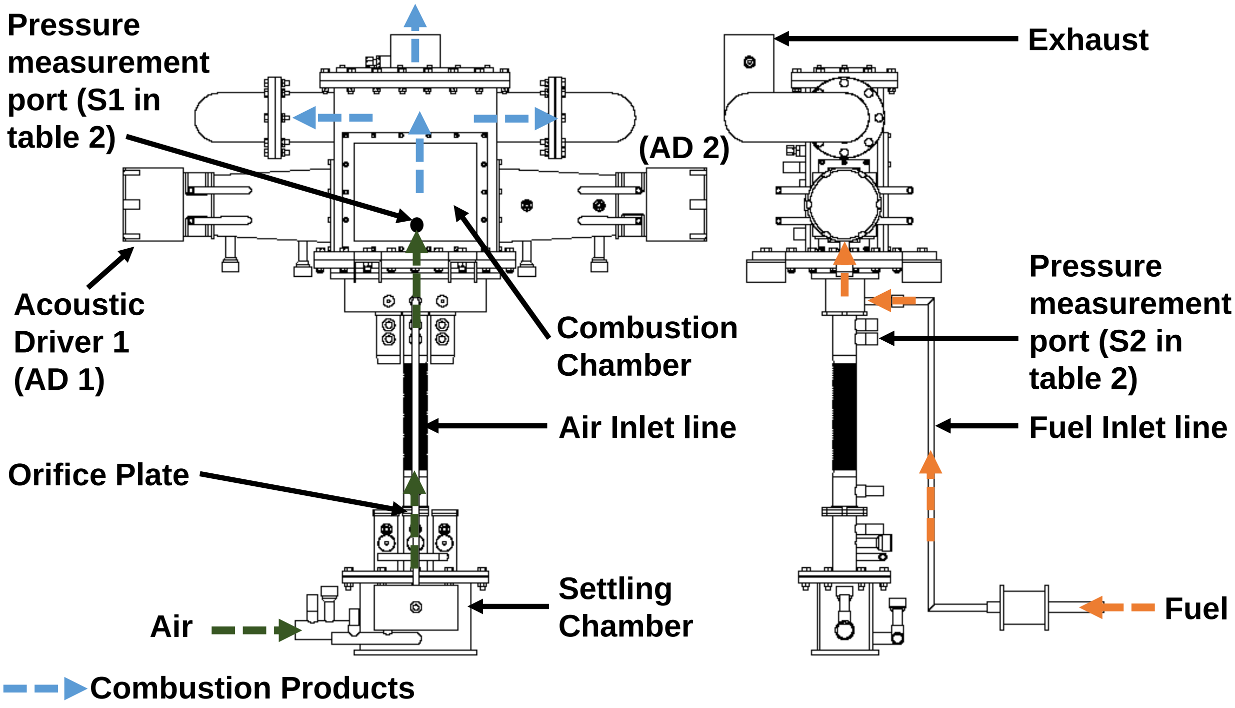

Figure 1: Experimental test rig indicating the flow path and all the important features.

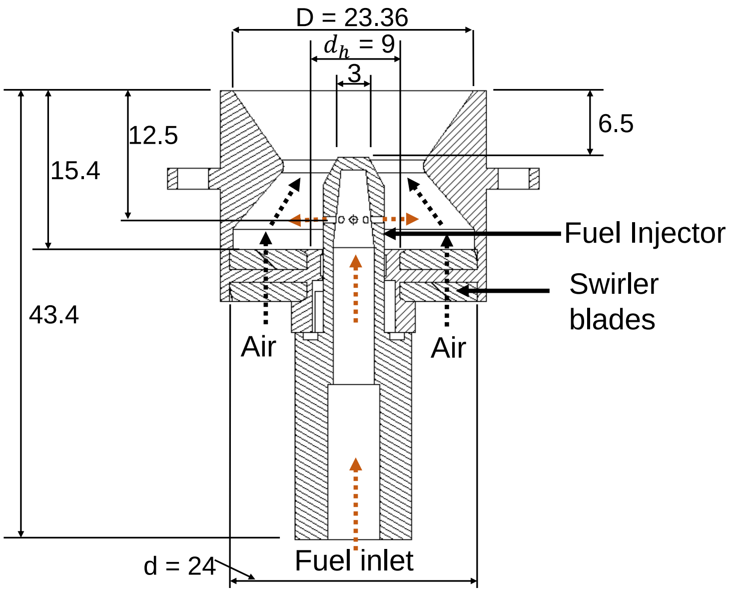

Figure 2: Sectional view of the injector assembly. The dotted orange and dotted black arrows represent the direction of the flow of fuel and air, respectively.

channel arbitrary function generator (make: Tektronix AFG2021) is used to generate the excitation signal (or perturbation signal) to an amplifier (make: Tonylee CS900) which amplifies the signal and sends to the two acoustic drivers. In this study, we have used only sinusoidal functions of the form - $Asin(\omega t + \phi)$ as input to the two acoustic drivers. Here, A is the signal amplitude in voltage, and ω is the angular frequency and ϕ is the phase of the sinusoidal wave. The locations of the high-frequency pressure sensors (PCB 113B28) placed at the back wall of the combustion chamber are given in the table 1.

Table 1: High-frequency pressure sensor location in the experimental test rig. x is the streamwise direction (positive along the flow); r is the radial direction (along the forcing direction; positive towards right); y is the other transverse direction.

Sensor	**x**	**y**	**r**
center of central injector at the dump plane	0	0	0
S1 (combustor back wall)	+12	-60	0
S2 (inlet line)	- 81.1	18.3	0

2.3. Details of the diagnostic techniques

In this work simultaneous high-repetition rate 2D-2C particle image velocimetry (PIV) in the streamwise midplane ($r - x$), line-of-sight integrated OH* chemiluminescence and pressure measurement are performed to undestand the dynamical response of a swirl-stabilized flame to external acoustic forcing.

Figure 3a shows the schematic of the optical arrangement for the simultaneous 2D-2C Particle image Velocimetry (PIV), line-of-sight integrated OH* Chemiluminescence in the streamwise midplane ($r - x$). Time-resolved 2D-2C particle image velocimetry (PIV) is performed to obtain in-plane velocity components. A high speed double-pulsed Nd:YLF (yttrium-lithium-fluoride) laser (make: Photonics Industries) at 527 nm is used to illuminate the PIV seed particles. The laser beam is passed through a sheet forming optics that forms a diverging laser sheet with a thickness of approximately 1 mm. The laser sheet enters through the top window of the combustion chamber for the measurements performed in the $r - x$ plane. The PIV measurements are performed at an acquisition rate of 5 kHz. A high-speed CMOS camera (Photron FASTCAM SA5) is used for acquiring the Mie scattered images from the seed particles. The scattered light is focused onto the camera sensor using a 105 mm Nikon lens. A band-pass filter at 527 nm with $FWHM$ of 10 nm is used to allow the Mie scattered light and suppress the background flame luminosity. The images are acquired at a resolution of 1376×1040 pixels in the frame straddling mode. The time delay between the two laser pulses (δ) is varied depending on the bulk flow velocity to obtain an optimum particle displacement. Due to strong interference from the laser scattering at the dump plane, the velocity field could not be computed up to 4 mm above the dump plane. The acquired images are processed using the LaVision Davis 8.4 software to compute the velocity vectors. A set of 100 background images are taken for every run. The mean background image is subtracted from each instantaneous time snapshot. The velocity vectors are computed using a multi-pass approach with interrogation window size decreasing from 64×64 pixels to 32×32 pixels, with a 50% overlap. This gives a vector resolution of 1.1 mm/vector. The uncertainty in the velocity field is computed using DaVis 8.4 using the correlation statistics method (34; 35). The uncertainty is computed in time-averaged velocity magnitude. The maximum value of uncertainty in the time-averaged velocity magnitude is 3.93% in the V-flame around the inner shear layer.

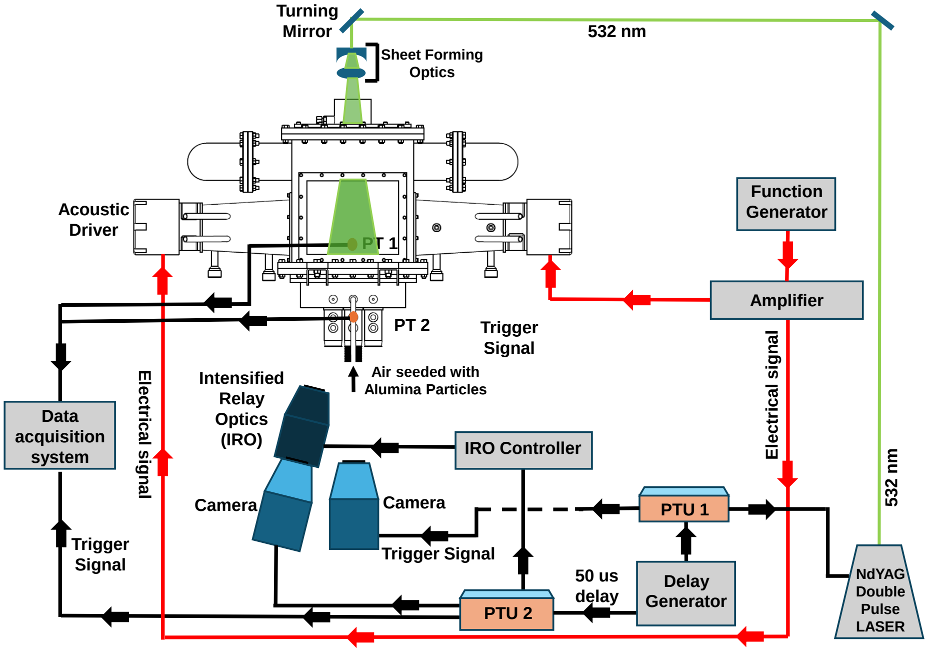

Figure 3: Schematic of the experimental test setup for simultaneous 2D-2C particle image velocimetry (PIV) in the streamwise midplane ($r - x$), line-of-sight integrated OH* chemiluminescence and pressure measurement.

A high-speed camera (Photron FASTCAM SA5) coupled with a LaVision image intensifier (Lavision high-speed IRO X) is used for time-resolved OH* chemiluminescence imaging. The gate and gain of the intensifier are set to 100 μs and 55 respectively. A 100 mm UV lens (CERCO) and an enhanced UV band-pass filter (310 ± 20 nm) are used to collect and focus the OH* chemiluminescence emission from the flame onto the camera. The OH* chemiluminescence is performed at an acquisition rate of 5 kHz.

The current study investigates the effect of transverse acoustic forcing over a partially-premixed swirl-stabilized methane/air flame. The flow Re and global equivalence ratio are kept constant at 3000 and 1.0, respectively. As the focus of this study is to understand the effect of high frequency transverse acoustic forcing at large amplitudes, a forcing frequency of 1500 Hz ($5T$ mode of the combustor geometry) is chosen. Figure 4 shows the acoustic eigenmodes computed for the combustion chamber indicating the 1T, 3T and 5T mode shapes. The modes indicates no noticeable acoustic interaction with the injector or the air feed manifold. Furthermore, to investigate the

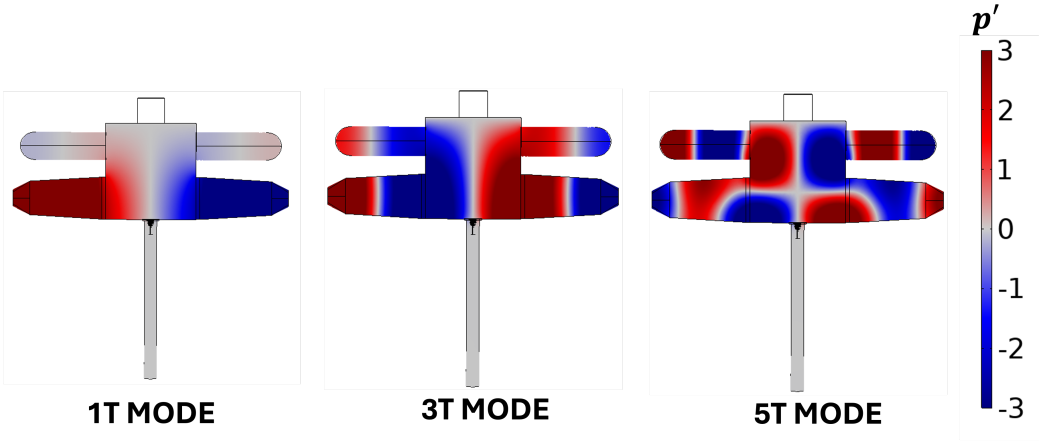

Figure 4: 1T, 3T and 5T acoustic eigenmodes computed for the combustor.

non-linear response of the swirl stabilized flames the forcing amplitudes are varied such that the pressure fluctuations measured at the location S1 during the reacting flow experiments varied from 1.6% to 5% of the chamber pressure (P_{ch} = 910 kPa). An in-phase forcing of the compressor driver is conducted to create a pressure antinode (PAN) at the injector. Table 2 shows the investigated acoustic amplitudes at a frequency of 1500 Hz. Both the speaker's parameters are adjusted to generate nearly similar pressure responses at the injector location.

Table 2: List of tested amplitudes and frequencies for the study; $P_{ch} = 910$ kPa

Case	**Frequency (Hz)**	**Amplitude % of P_{ch}**	**Condition** PAN/VAN
$CaseA$	1500	1.6	PAN
$CaseB$	1500	2.7	PAN
$CaseC$	1500	2.9	PAN
$CaseD$	1500	4.6	PAN
$CaseE$	1500	5.0	PAN

3. Results and discussions

The experimental observation of the effect of transverse acoustic forcing on swirl-stabilized $CH_4 - air$ flame at a frequency of 1500 Hz at different forcing amplitudes are discussed in the following section. Again, the flow Reynolds number $Re = 3000$, geometric swirl number $SN_G = 1.049$, and the equivalence ratio $(\phi) = 1.0$ are kept constant for all the experiments.

Figure 5a and b shows the time averaged streamwise (u_x) and spanwise (u_r) velocity fields overlaid on the velocity vectors and figure 5c shows the time-averaged OH* chemiluminescence intensity field for the unforced swirl-stabilized partially premixed methane-air flame. The flow-field features a large central recirculation zone (CRZ) surrounded by high velocity annular jet. The flame is stabilized between the shear layers of the annular jet and the CRZ. During the unforced state, the average flame-shape is a V-shaped flame.

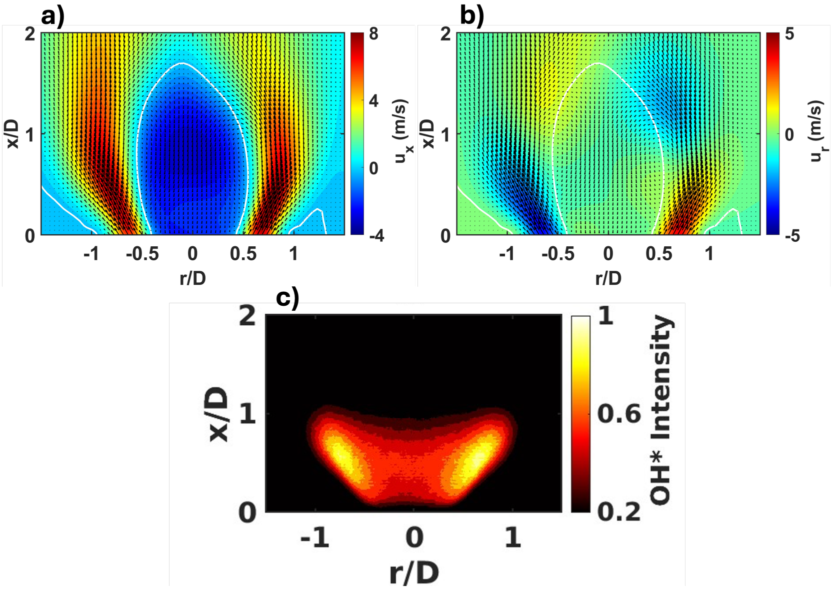

Figure 5: Time-averaged (a) streamwise velocity (u_x), (b) spanwise velocity (u_r), and (c) OH* chemiluminescence intensity of the unforced swirl-stabilized partially premixed methane-air flame at $Re = 3000$, $SN_G = 1.049$ and $\phi = 1.0$.

3.1. Effect of in-phase transverse acoustic forcing: Acoustic field response

The experimental observations of the effect of transverse acoustic forcing over swirl flame under different forcing conditions are discussed in the following sections. The system response us due to the coupled interactions between the turbulent-reacting flow and the acoustics. In-phase acoustic forcing at a frequency of 1500 Hz induces velocity oscillations that in turn affects the hydrodynamics of the swirling jet. The perturbation in the flow hydrodynamics in turn affects the flame surface area through vortical interactions at the forcing frequency, causing a heat release response. First, we discuss the response of the acoustic field measured inside the combustor to forcing amplitudes. Figure 6 shows the acoustic field response of the swirl-stabilized flame to the external acoustic forcing as a function of forcing amplitude. As the amplitude of forcing frequency is varied, the combustion chamber pressure fluctuations varies from 1.6% - 5.0% of the chamber pressure (P_{ch}). Case A exhibits the lowest acoustic field amplitude of 1.6% and the acoustic response appears relatively stable and periodic, indicating a predominantly linear response of the flame to the imposed acoustic field. The pressure amplitude also shows a continuous growth with time indicating a positive feedback with the flame. As the forcing amplitude increases, Case B and C exhibit signs of intermittency, characterized by repetitive modulation of the pressure amplitude. One of the key features of the pressure signal in Case B and C is a dip in the amplitudes once the pressure oscillation exceeds a threshold. This behavior could indicate a non-linear interactions or mode switching in the flame dynamics of the swirl-stabilized flame. Case D demonstrates a pronounced form of intermittency characterized by sudden drops in amplitude followed by bursts of oscillations, reflecting higher degree of non-linear interactions. In the case showing 5.0% of pressure oscillation (Case E), the response appears more intense but somewhat irregular, leading to the flame approaching a limit of stability eventually blowing-off. Thus, with an increase in forcing amplitude the swirl-stabilized flame exhibits dynamical blow-off due to strong acoustic-hydrodynamic-heat release interactions. Although the initial states of all the flames are identical, with an increase in forcing amplitude the dynamical states of the flame vary significantly exhibiting possible bifurcation from a linear periodic flame response to an onset of repetitive intermittency of low and high amplitude oscillations. These transitions highlight the increasing influence of non-linear effects as the forcing amplitude grows.

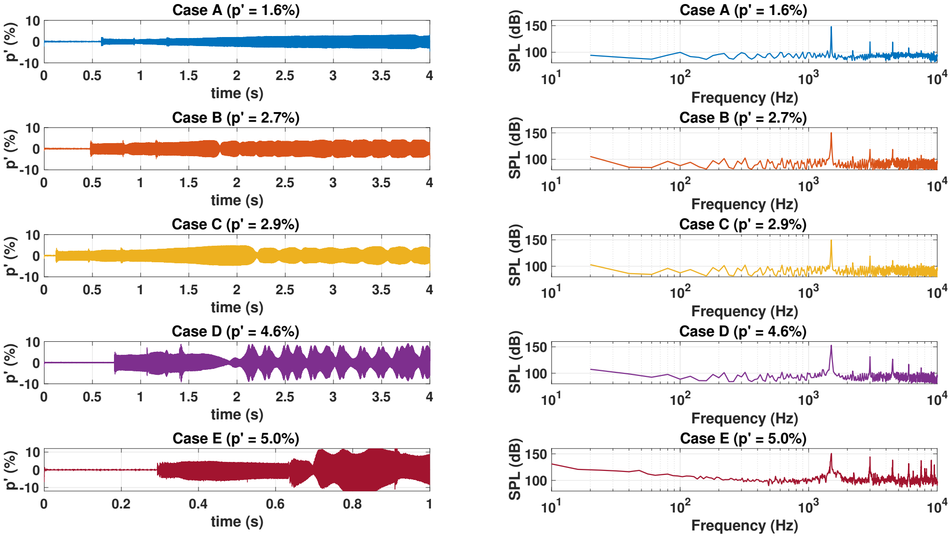

Figure 6: (Left column) Unsteady pressure response of the swirl-stabilized partially premixed methane-air flame at amplitudes - (1.6%, 2.7%, 2.9%, 4.6% and 5.0%), and (Right column) the corresponding power spectral density at all the forcing amplitudes; $Re = 3000$, $SN_G = 1.049$ and $\phi = 1.0$.

3.1.1. Continuous wavelet transform

Figure 7 shows the spectrograms of the continuous wavelet transform (CWT) of the pressure signals providing a time-frequency representation of the dynamic response of the swirl-stabilized flame to external acoustic forcing. Across all five cases, the CWT reveals how the energy distribution around the forcing frequency (1500 Hz) evolves with increasing pressure amplitude. At low forcing (Case A), the response is steady and localized in frequency, indicating a linear and coherent behavior. As the forcing amplitude increases (Cases B and C), the CWT shows signs of amplitude modulation and slight spectral broadening, suggesting the onset of non-linear interactions. In Case B some intermittent modulation in the pressure amplitude begin to surface, indicating possible early signs of non-linearity or interaction with other flame dynamics. However, the structure remains mostly coherent. For Case C the wavelet spectrum begins to show visible amplitude modulation and spreading in frequency. The spectrogram shows intermittency and brief dropouts in oscillation strength. These signatures point toward non-linear coupling between the acoustic field and flame dynamics. The system might be near a bifurcation point where small changes in amplitude cause noticeable spectral change. In higher forcing regimes, particularly, in Case D, the CWT highlights pronounced intermittency, with bursts of high energy interspersed with quiet periods, whereas the spectral energy spreads over a broader band near 1500 Hz. This irregular energy bursts hallmarks strong non-linear dynamics and transition towards flame blow-off. The flame ultimately blows-off with further increase in forcing amplitude in Case E. Overall, the CWT effectively captures both steady and transient features of the pressure signal, offering insight into the stability of the flame and the nature of acoustic–flame coupling.

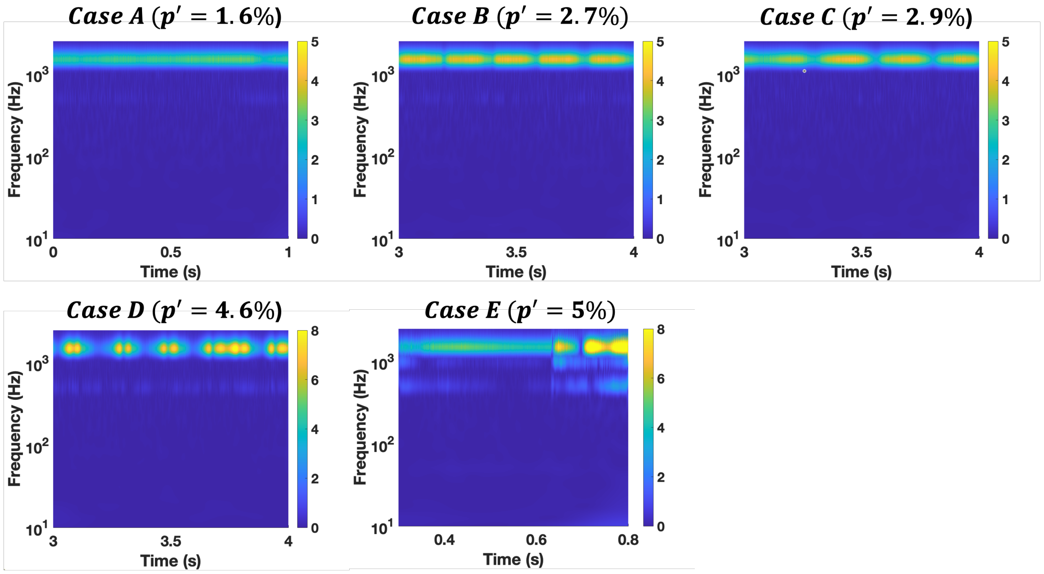

Figure 7: Continuous wavelet transform spectrogram of the unsteady pressure at all the forcing amplitudes - (1.6%, 2.7%, 2.9%, 4.6% and 5.0%), indicating the response of the swirl-stabilized partially premixed methane-air flame to high frequency transverse acoustic forcing.

3.1.2. Transition in system dynamics: Phase- space-trajectory

To further analyze the underlying dynamics of the pressure fluctuations, the time series is embedded into a higher-dimensional phase space using time-delay embedding. According to Takens' theorem, a dynamical system can be reconstructed from a single scalar time series by forming delay vectors:

$$\mathbf{X}(t) = [x(t),\ x(t+\tau),\ x(t+2\tau)]$$

where τ is the time delay, and $x(t)$ is the pressure signal. The appropriate value of τ is selected which quantifies the statistical dependence between $x(t)$ and $x(t+\tau)$. A critical step in reconstructing the phase space from a time series is to select an appropriate time delay τ. Rather than using an arbitrary or fixed value, a data-driven approach based on mutual information (MI) is employed. Mutual information quantifies the statistical dependence between the signal $x(t)$ and its time-delayed counterpart $x(t+\tau)$:

$$\mathrm{MI}(\tau) = \sum_{i,j} p_{ij}(\tau) \log \left(\frac{p_{ij}(\tau)}{p_i p_j} \right)$$

where $p_{ij}(\tau)$ is the joint probability of $x(t)$ and $x(t+\tau)$ falling into bins i and j, and p_i, p_j are their marginal probabilities. Unlike autocorrelation, mutual information captures both linear and non-linear dependencies. The optimal delay τ_{opt} is chosen as the first local minimum of the MI curve:

$$\tau_{\mathrm{opt}} = \arg\min_{\tau} \mathrm{MI}(\tau)$$

This delay minimizes redundancy between coordinates in the reconstructed state space while retaining dynamic information. It ensures that successive coordinates are sufficiently independent for proper unfolding of the attractor. Furthermore, the trajectories are time colored, which in a phase space trajectory involves assigning a color gradient to each point along the reconstructed trajectory based on its temporal position in the signal. This visual technique overlays temporal progression on the spatial dynamics of the system, helping to identify how the system evolves over time in its state space. Early points appear in darker shades, while later points appear in lighter shades. This reveals not just the shape of the attractor but how the system moves through it. The reconstructed phase-space trajectories for Cases A to E reveal a clear progression in the system behavior as the acoustic forcing amplitude increases. In Case A, the trajectory forms a compact and regular orbit, indicating a stable, periodic response. The flame and pressure dynamics are well-synchronized and repeat consistently. As the amplitude increases in Cases B and C, the trajectory begins to stretch and fold, showing signs of quasi-periodicity and the onset of non-linear interactions. Case C, in particular, the phase space becomes more complex, with folded and branching structures. Time coloring highlights irregular movement—some regions evolve slowly (denser color clustering), others more quickly. This indicates the onset of intermittent dynamics and non-linear coupling. For Cases D and E, the phase space becomes increasingly irregular and high-dimensional, reflecting a transition into a complex, possibly chaotic regime. Time coloring shows non-uniform progression — rapid changes (color jumps) alternate with slow evolution. This reflects strong non-linearity, possible chaotic behavior, and unstable flame dynamics. For Case E, the attractor is highly scattered and fragmented, with no clear looping. Time coloring reveals bursts of motion and stalling, indicating intermittency and possible transient events like flame detachment or local extinction. The phase-space trajectory suggests that the system is near or beyond a bifurcation point, entering a chaotic or blow-off-prone regime. Furthermore, this is corroborated by the analysis of phase velocity. Once the trajectory is reconstructed in 3D, the phase velocity of the system is calculated as the magnitude of the rate of change of state:

$$v(t) = \left\| \frac{d\mathbf{X}(t)}{dt} \right\| = \sqrt{\left(\frac{dx}{dt}\right)^2 + \left(\frac{dy}{dt}\right)^2 + \left(\frac{dz}{dt}\right)^2}$$

where $x(t)$, $y(t) = x(t+\tau)$, and $z(t) = x(t+2\tau)$. This velocity quantifies how rapidly the system evolves through its phase space.

Figure 9 which shows low, steady values in A but increasingly large and erratic spikes in D and E—suggesting bursts of rapid dynamical evolution, associated with unsteady flame dynamics or near-blow-off behavior. These patterns strongly indicate a dynamical bifurcation or route to chaos as the system is pushed into a more non-linear state by higher acoustic forcing.

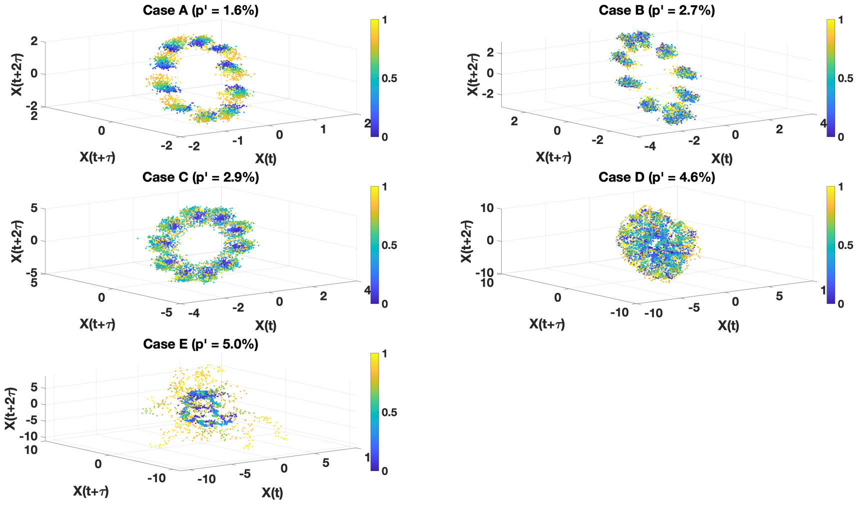

Figure 8: Time colored phase-space trajectory computed for the unsteady pressure at all the forcing amplitudes indicating the variation in the dynamical state of the swirl-stabilized partially premixed methane-air flame due to high frequency transverse acoustic forcing.

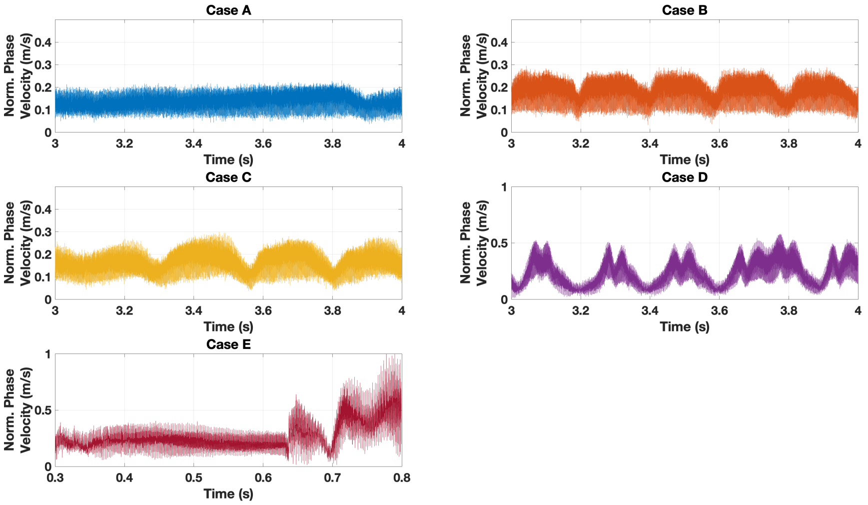

Figure 9: Variation of phase velocity in the phase-space trajectory computed for the unsteady pressure with an increase in forcing amplitude.

3.1.3. Bifurcation Analysis

The Poincaré section-based method for obtaining a bifurcation plot involves tracking the local pressure maxima in the time series of the system's response as a function of a control parameter—in this case, the acoustic forcing amplitude. For each pressure signal corresponding to a given forcing amplitude, the local maxima are identified using peak detection technique. These maxima represent discrete points where the system reaches a turning point in its oscillatory cycle and serve as a reduced-dimensional snapshot of the underlying dynamics. By plotting these local maxima against the corresponding forcing amplitudes, a bifurcation diagram is constructed. This diagram reveals how the system transitions from periodic (single-valued maxima) to quasi-periodic or modulated (multiple-valued) and eventually to chaotic or intermittent behavior (broad, irregular distribution of peaks) as the forcing increases. The Poincaré-based bifurcation plot thus provides a clear and intuitive visualization of the non-linear transitions and dynamic regimes present in the flame–acoustic interaction. Figure 10 shows the bifurcation plot created using the Poincaré section based on local maxima of the pressure signals. The control parameter in the current study is the forcing amplitude which is measured in terms of the flame acoustic response measured in the combustion chamber. At low forcing (1.6%), the system exhibits a narrow variation in dominant peak per cycle, indicating a stable, periodic response. As the forcing amplitude increases $(2.7-2.9\%)$, the pressure peaks begin to spread, suggesting the onset of amplitude modulation. At higher amplitudes $(4.6 - 5\%)$, the local maxima become widely scattered, reflecting a loss of coherence and the emergence of strongly non-linear dynamics, including highly intermittent behavior. This progression of peak structure with increasing forcing illustrates a classical bifurcation scenario, where the flame transitions from periodic to modulate amplitude phase and ultimately exhibiting disordered behavior similar to flame blow-off. This highlights the complex coupling between acoustic forcing, flow hydrodynamics and flame dynamics.

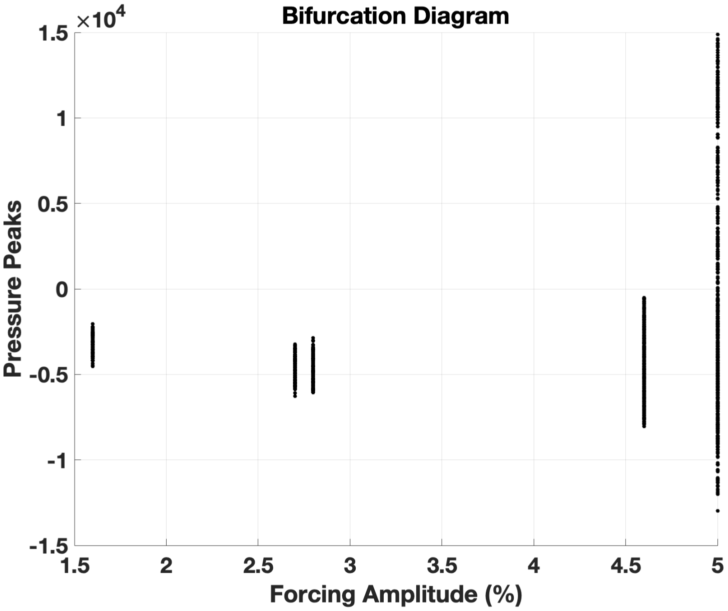

Figure 10: Experimental bifurcation plot for the swirl-stabilized partially premixed methane-air flame at $Re = 3000$, $SN_G = 1.049$, $\phi = 1.0$, indicating a bifurcation with an increase in forcing amplitude.

3.1.4. Recurrence Analysis of Pressure Signals

Recurrence plots (RPs) are powerful graphical tools used to visualize the times at which a system revisits the same or similar states in its phase space. Given a time series $x(t)$, the recurrence plot is defined as:

$$R_{i,j} = \Theta(\varepsilon - \|x_i - x_j\|), \quad i, j = 1, \ldots, N$$

where Θ is the Heaviside function, ε is the distance threshold, and N is the number of points, in the current analysis a threshold value of 10% of the diameter of the attractor is chosen. $R_{i,j} = 1$ indicates a recurrence between states x_i and x_j, while 0 indicates no recurrence. The result is a symmetric binary matrix that reveals dynamic patterns such as periodicity, drift, intermittency, or chaos. Recurrence plots are denoted by black and white lines, where the black lines denote two points are sufficiently close by in the phase-space and hence, the recurrence of the phase-space trajectory. Figure 11 shows recurrence plots for the pressure signals with increasing acoustic forcing amplitudes. Similar to, earlier analyses where the pressure fluctuations for Case A was found to be periodic indicating coherent behavior, the RP for Case A clearly exhibits a dynamics attributed to periodic oscillations. The black lines are found to be equally spaced, continuous and parallel to the main diagonal. The regular, repetitive diagonal lines are indicative of stable, periodic behavior with high predictability. The RP computed for Case B and Case C indicate onset of intermittency in the periodic oscillations as shown in figure 11b and 11c. The dense black patches on the RPs correspond to states of periodic oscillation or laminar states in the system. Furthermore, the density of the black region reduces with increased regions of white. This indicates that the laminar states are encountered with regions of modulated amplitudes which are still oscillatory. But the system dynamics is such that the recurrence of phase space trajectories is significantly reduced. This can be seen clearly by comparing the CWT scalogram plots of Case B and C of the pressure oscillation time-series in figure 7b and 7c. This behavior is suggestive of early signs of non-linearity in the response of the swirl stabilized flame with an increase in forcing amplitude. The RP structure resembles a square with elongated corners. This kite-like elongated structures seen for both Case B and C are characteristic of type II intermittency (36). Klimaszweska and Zebrowski, presented an analysis and compared intermittency types based on the recurrence plot analysis. Types II and III were found to have similar large-scale patterns of black squares. However, a closer look indicated that the kite-like structure differentiates type II from type III. Accordingly, the recurrence plot obtained for the Cases B and C oscillations in this system indicates a type II intermittency. Furthermore, the intermittent behavior of intermittency itself changes with a change in the control parameter. In an earlier study (37), it is shown that as one varies the control parameter further from the bifurcation point for intermittency, the intermittent bursts appear more frequently. For Case D, figure 11d shows that beyond the point of bifurcation, further variation in intermittency is observed with an increase in forcing amplitude. Here, the RP becomes more fragmented with short diagonals and vertical segments, indicating transient trapping and complex dynamics. The local dynamics are non-stationary indicating frequent bursts of intermittent oscillation. Case E sees a flame blow-out with further increase in forcing amplitude and prior to the blow out the RP indicates largely scattered structure of high entropy, consistent with chaotic or blow-off-prone behavior. Table 3 summarizes quantitative values of recurrence analysis for Cases A-D. The recurrence rate decreases with increase in forcing amplitude consistent with the qualitative observations based on the recurrence plots. Long continuous diagonal indicates a deterministic behavior and as the longest diagonal becomes shorted system becomes intermittent and more chaotic. Quantitatively, recurrence analysis confirms that the swirl-stabilized flame transitions from a predictable state to an intermittent and more chaotic state.

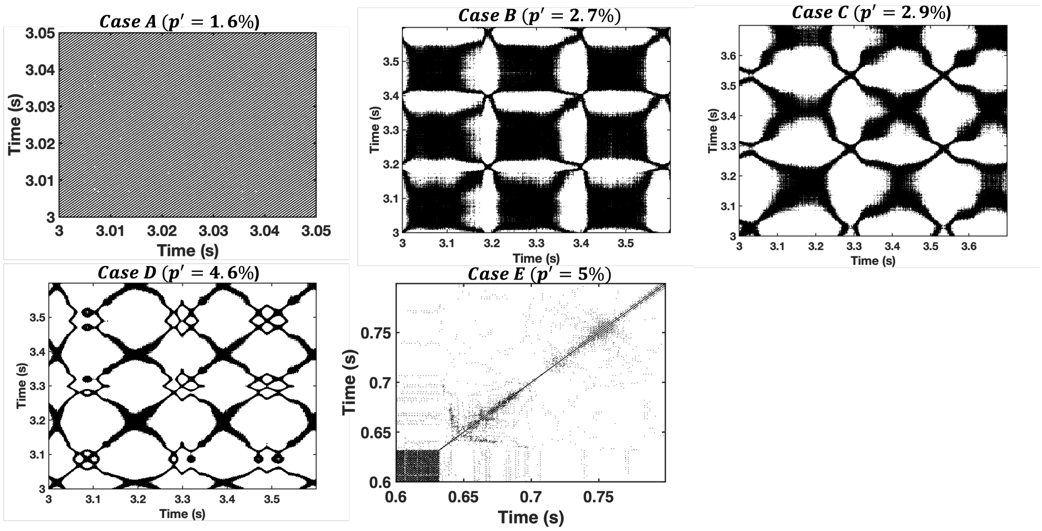

Figure 11: Recurrence plots (RPs) highlighting the state of the partially premixed swirl-stabilized flame transitioning from a linear periodic response (Case A) to onset of intermittency (Case B and C) to bursts of strong intermittency and chaotic response (Case D and E).

Table 3: Quantitative recurrence analysis during the intermittent phase of all the cases.

Cases	**Recurrence Rate**	**Determinism**	**Longest Diagonal**	**Entropy**
Case A	3.051	84.0	772	3.55
Case B	0.872	76.0	543	4.24
Case C	0.389	72.5	412	4.35
Case D	0.282	70.2	193	4.81

Thus, with the help of RP it is possible to understand the dynamical response a swirl-stabilized flame to high frequency large amplitude acoustic forcing. A lower forcing amplitude the flame responds coherently with a periodic oscillation followed by an onset to a Type-II intermittency where the system dynamics encountered sudden loss in recurrence in the phase-space trajectory. At higher forcing amplitudes the system dynamics is further affected in a manner that increases the intermittency with the RP showing frequent bursts of intermittent oscillations followed by a largely scattered RP indicative of the flame undergoing blow-off. This method effectively complements phase-space, bifurcation, and wavelet analyses in capturing the non-linear dynamics of combustion instabilities.

3.2. Effect of in-phase transverse acoustic forcing: Flow and Flame response

3.2.1. Flame shape transition

The acoustic field measured in the combustion chamber shows presence of a complex interaction between the acoustic forcing, hydrodynamics and flame heat release. The system exhibits a Type-II intermittency at larger forcing amplitudes which is a precursor to flame blow-off. These behavior are further investigated by plotting the transition in flame shapes during these variation in the system dynamics. Figure 12 shows the pressure oscillations measured at the combustor mid-plane and the corresponding average flame shape attained during a time duration highlighted in red dashed box. The states of the flames are defined as unforced, forced and intermittent states. For example, B_{Un}, B_F and B_{Int} represent the unforced, forced and intermittent states of the flame for the Case B. The unforced state of the flame exhibits a V-shaped swirl-stabilized flame. Figure 12a shows the time averaged flame shape obtained within the region of interest highlighted by the red dashed box for the unforced and forced states of the flame. It is evident that at lower forcing amplitudes (1.6%) there is no distinct variation in the flame shape seen for Case A and it remains a V-shaped flame. At higher forcing amplitudes, Case B and C ($2.7 - 2.9\%$), the forced stated of the flame is found to have a shorter flame length which spreads radially outwards, forming a wide V-shaped flame, as compared to the unforced V-flame state. The pressure time-series shows that when the in-phase acoustic forcing is turned-on the pressure amplitude shows a growth with time until it shows a dip in the amplitude. The first dip in amplitude is associated with the change in flame shape to wide V-shaped flame. The transition into this compact flame state is gradual and is found to be dependent on the evolution of the pressure amplitude with time. The modulation in the pressure field during the intermittent phase is associated with the variation in the flame shape between the V-shape and wide V-shaped flames. Case D exhibits the most interesting observation, when the system undergoes bifurcation and a state of frequent bursts of intermittent oscillations are observed. The forced state of the flame shows an even shorter flame and wider flame state. However, this state of the flame may not be a stable state because the system quickly transitions and enters in to frequent high amplitude bursts of intermittent oscillations. During the peak of the intermittent bursts of oscillation the flame is observed to transition to a wall-flame state and it oscillates between wall-flame state and wide V-flame state over one cycle of high and low amplitude oscillations. Based on the pressure response during a burst of intermittent oscillations, it can be hypothesized that the coupling between the pressure fluctuations and intensity fluctuations for the wall-flame state is very high. In Case E, discussed in subsequent section, once the flame transitions to the wall-flame state it blows-off.

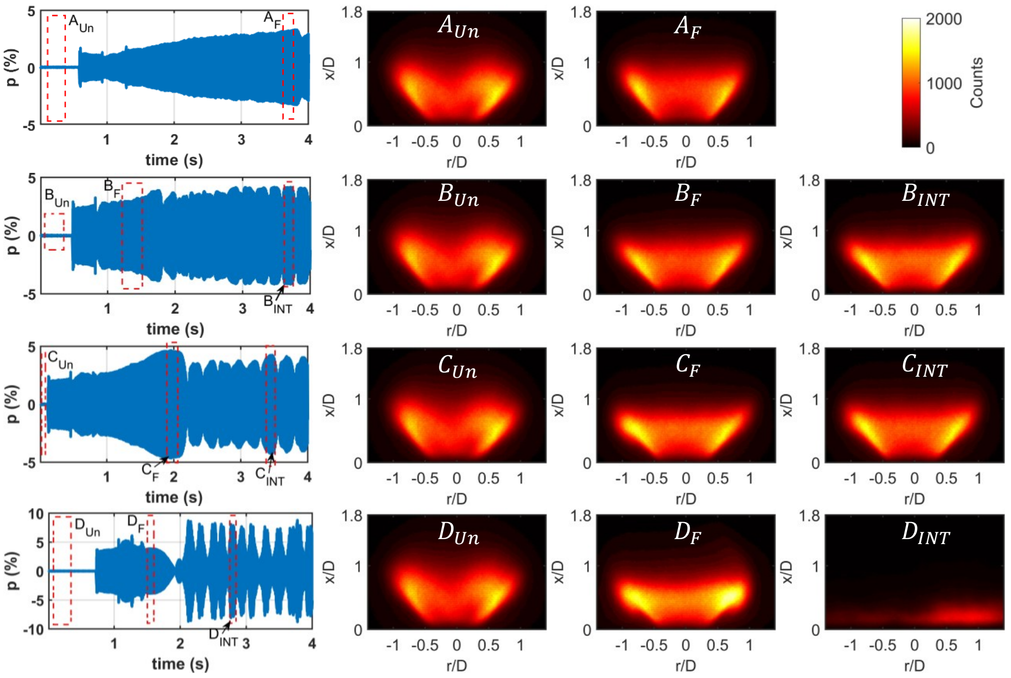

Figure 12: Time-series of unsteady pressure measurements with regions marked as unforced (A_{Un}, B_{Un}, C_{Un} and D_{Un}), forced (A_F, B_F, C_F and D_F) and intermittent (B_{INT}, C_{INT} and D_{INT}). The rows represent Cases A-D. Each unsteady pressure time-series shows corresponding time-averaged OH* chemiluminescence intensity averaged at the time instances marked as unforced, forced and intermittent.

Case D shows the highest levels of intermittency and the associated reason is the continuous transition in the flame shape from V-shaped to wider V-shape to a wall-flame state. Figure 13 shows the instantaneous images of the flame for the unforced state, forced state and after the onset of intermittent high and low amplitude oscillations. During the intermittent phase the fluctuations in the area averaged OH* intensity strongly correlates with the oscillation in the pressure field. Here four different events are discussed, where $E1$ captures the unforced flame and forced flame response immediately after turning on the in-phase forcing. The flame images before ($t = 0.7s$) and after forcing ($t = 0.8s$) do not show a significant variation in the flame shape. $E2$ captures small variation in pressure and OH* intensity captured between time, $t = 0.95 - 1.5s$. At $t = 1.099s$ the flame is found be a compact wider V-shaped during which there is small jump in the OH* intensity while a dip in the pressure field is observed. Furthermore, the flame is observed to lift-off at $t = 1.033s$ and $t = 1.413s$ during which a corresponding dip in the OH* intensity field is observed. These events that create a minor changes in the intensity and pressure field are found to be the precursor to the transition to the intermittent oscillation state. $E3$ captures an important transition where the pressure field shows a gradual drop in the amplitude of the pressure oscillation, attaining a minimum at $t = 1.9s$ and marking for the onset of intermittent behavior. The pressure oscillation further increases with an observed intermittent modulation in the magnitude of the amplitude. During this time the flame is observed to have transitioned to a compact wider V-type flame as seen at $t = 1.85s, 1.919s$ & $1.983s$. Furthermore, event $E4$ captures one cycle of intermittent burst in pressure and OH* intensity fluctuation between time $t = 3.175 - 3.432s$. It is evident that the flame retains the wider V-type flame shape during low amplitude pressure oscillation at $t = 3.197s$ and during the high amplitude oscillations the flame has transitioned to a wall-flame state which is also marked by a dip in OH* intensity field. The flame in the wall-flame state might be susceptible to blow-off, however at $t = 3.301s$, there is a small increase in the intensity creating a small dip in the amplitude of pressure oscillation. The twin peaks observed during a single burst of intermittent oscillation is indicative of major extinction and re-ignition events while in the wall-flame state.

3.2.2. Flow-flame interaction

Simultaneous $2D - 2C$ PIV, OH* chemiluminescence and unsteady pressure measurements are performed for Case D and E. Figure 14c) and d) shows the time-averaged and rms axial and radial velocity field of the react-

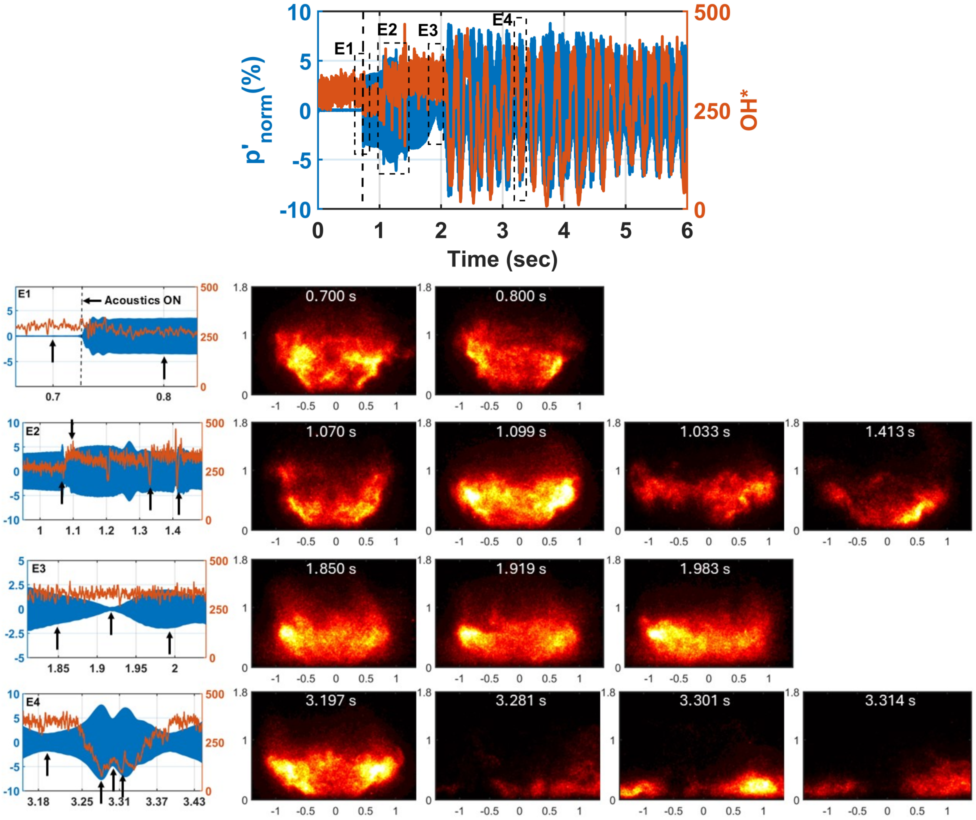

Figure 13: (a) Time series of pressure variation and spatially-averaged (entire field-of-view) OH* chemiluminescence, (b) zoomed-in section of figure (a) marked as events E1, E2, E3 and E4 showing occurrences of events observed in Case D, highlighting the state of the flame during the intermittent burst of oscillation.

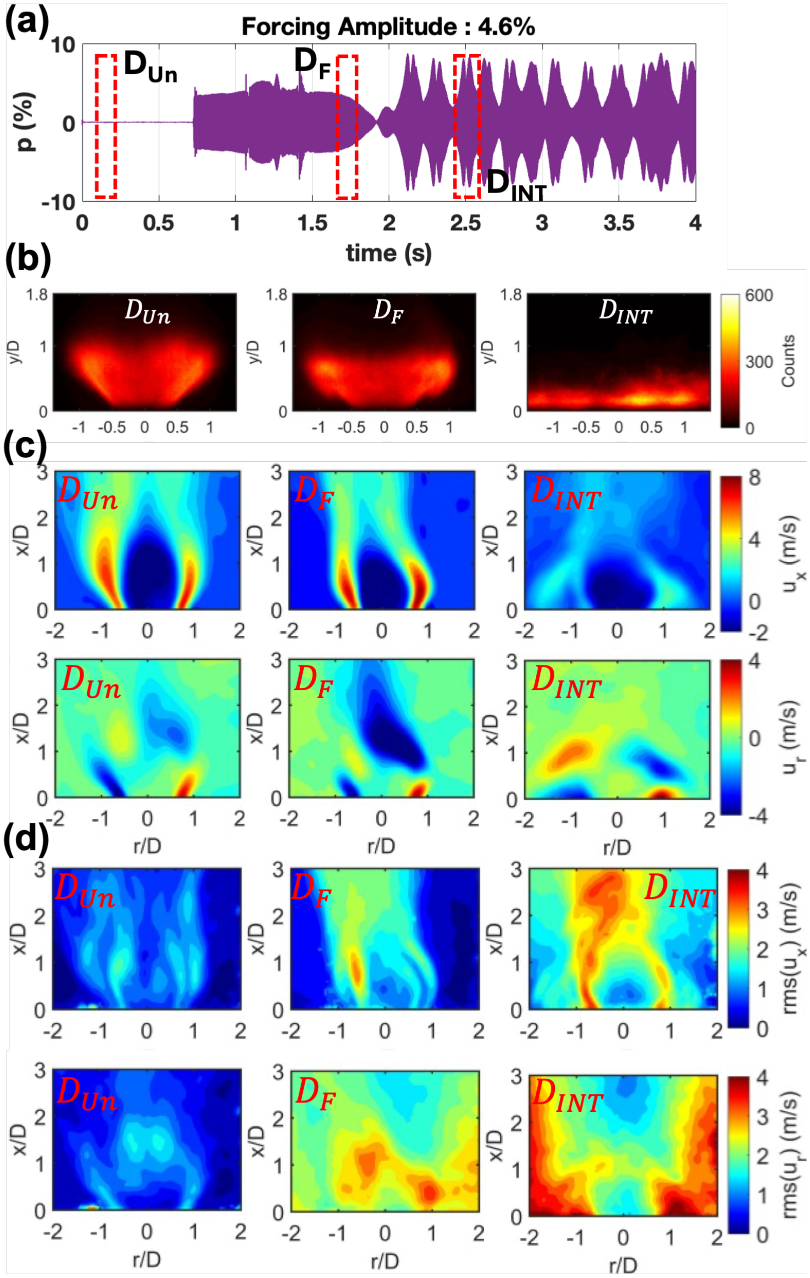

Figure 14: (a) Time series of the pressure oscillation measured for Case D, (b) rms of the OH* intensity field during the unforced (D_{Un}), forced (D_F) and intermittent oscillation (D_{INT}), (c) time-averaged streamwise (u_x) and radial (u_r) velocity field measured during the unforced, forced and intermittent oscillation, and (d) rms of the streamwise and radial velocity field measured during the unforced, forced and intermittent oscillation.

ing swirling jet for Case D. The unforced flow-field shows a large CRZ with the annular jets around it. The time averaged flow-field from the ROI D_F shows a relatively smaller and compact CRZ during the in-phase transverse acoustic forcing. The axial and radial velocity shows a significant increase in rms velocities induced by the in-phase transverse acoustic forcing. At higher amplitude oscillation as seen in Case D, the swirl-stabilized flame develops intermittency when the pressure field shows high and low amplitude oscillations. During one such intermittent burst of oscillation marked by ROI D_{INT}, the time-averaged axial and radial velocity field shows a wider CRZ, the time average radial velocity field shows the flow transitions between a wide BVB jet and a wall-jet (WJ), correspondingly, the flame oscillates between a wide-V-flame and the wall-flame state. The axial and radial velocity rms field shows a further jump in the rms velocity. The intermittency developed in the system dynamics is associated with the transition in the average flow and flame shapes of the swirl-stabilized flame.

Figure 15 shows instantaneous OH* intensity and streamwise velocity (u_x) contour at different instants in time during one burst of intermittent high and low amplitude oscillation. The flame is observed to transition from a V-flame to a wider V-flame to a wall-jet flame and back to a V-flame. At the beginning of the intermittent burst, the flame is wide and compact (figure 15(a1)). In the streamwise u_x velocity contour, an outwardly curved annular jet and a central recirculation bubble (CRB) is observed (figure 15(b1)). Gradually the flame becomes more wider and compact (figure 15(a2)) and correspondingly the annular jet shifts away from the centerline (figure 15(b2)). Next, the flame transitions to the wall-jet flame (figure 15(a3 - a5)), and the flow is observed to be in the wall-jet flow state with a large central recirculation bubble (figure 15(b3 - b5)). And later while the acoustic excitation is still ON, the flame returns to the wider V-flame (figure 15(a7)).

This intermittent oscillation cycle repeats multiple times. Thus, it can be concluded that during a burst of intermittent pressure oscillation the swirling jet transitions from a bubble-type vortex breakdown (BVB) to a wall jet (WJ) state. Correspondingly, the flame follows the flow and transitions from a V-shaped flame to a wall-flame state. Therefore, the mechanism for the transition in the flame shape is mainly due to the transition in the base flow of the swirl jet due to the induced velocity oscillations. A similar observation has been reported by Gupta et al. (38) where an isothermal swirl jet transitions from a columnar jet with a BVB to a wall jet state with a wide open vortex breakdown state when forced by an in-phase transverse acoustic

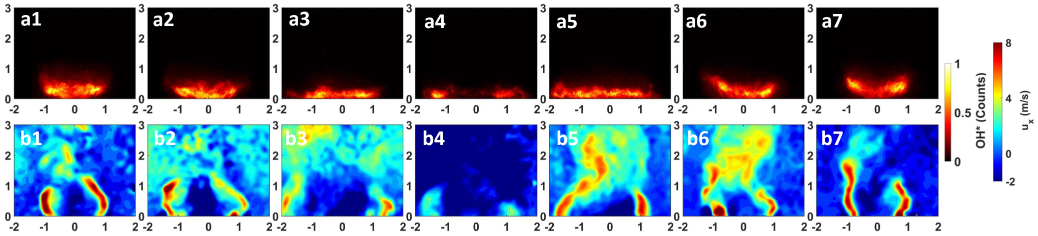

Figure 15: (First row) Instantaneous OH* intensity, and (second row) streamwise velocity (u_x) contour at different instants in time during one oscillation cycle of transition from V-flame to wall-jet flame and back to V-flame as captured in Case D.

field. The authors hypothesized that the in-phase transverse acoustic field induces a strong radial velocity oscillation near the jet shear layer. When these radial velocity fluctuations exceed a critical threshold it deflects the shear layers transitioning from a columnar jet (CJ) to a wall-jet (WJ).

Figure 16 shows simultaneous variation of OH* intensity and streamwise velocity (u_x) extracted from the inner shear layer region centered at $x/D = 0.6; r/D = 0.6$. During the intermittent bursts of high and low amplitude pressure oscillations, it is observed that the streamwise velocity field (u_x) extracted from $L1$ oscillates between positive and negative value. The u_x has positive values when the OH* intensity is high, indicating that the flame is in V-shape and the flow field is in columnar-jet state (CJ). And when the u_x has negative values the OH* intensity is low (or close to zero) indicating that the flame is in wall-flame state and the flow is in wall-jet flow state (WJ). This transition of the flame between V-flame and wall-jet flame is coupled to the variation in the velocity field response to the transverse acoustic forcing. Therefore, the flame response is primarily driven by the response of the flow-field to the in-phase external transverse acoustic excitation.

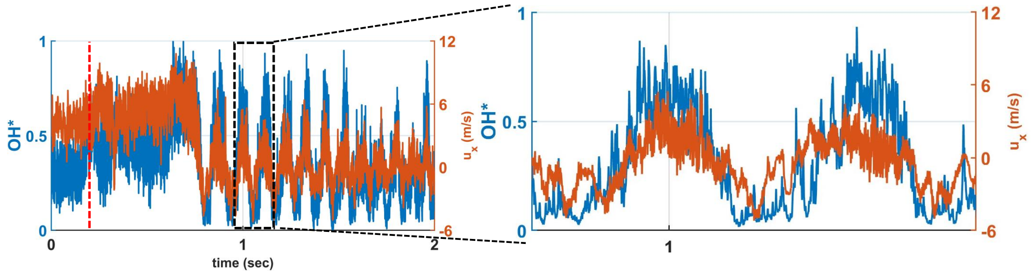

Figure 16: Left: Variation in the OH* intensity and streamwise velocity (u_x) with time extracted from the inner shear layer region ($x/D = 0.6; r/D = 0.6$) (a) for Case D. The red dotted line marks the instance when the acoustics is turned ON; Right: zoomed-in view around $1s$.

3.2.3. Cross wavelet transform analysis (XWT)

The XWT provides a powerful method to analyze the joint time–frequency behavior between two time series. The cross wavelet transform between the pressure fluctuations, $p'(t)$ and the intensity fluctuation, $I'(t)$, is defined as:

$$W_{p'I'}(s,t) = W'_p(s,t) \cdot W^*_{I'}(s,t)$$

where, $W'_p(s,t)$ and $W_{I'}(s,t)$ are the continuous wavelet transforms of $p'(t)$ and $I'(t)$ at scale s and time t, $(\cdot)^*$ denotes the complex conjugate. The magnitude $|W_{p'q'}(s,t)|$ indicates the local covariance in time-frequency space, while the phase of $W_{p'q'}(s,t)$ encodes the relative phase between the two signals. The $W_{pq'}(s,t)$, explains time-localized coupling between pressure and heat release oscillations, the frequency range of strong interaction, and phase synchrony and lead–lag relationships using phase arrows. These features are crucial for diagnosing the onset of thermo-acoustic instabilities and for designing effective control strategies. Figure 17(a-e) shows the XWT scalograms between pressure and flame intensity for the Cases A-E, respectively.

The XWT of Case A shows a strong, narrow-band response at the forcing frequency of 1500 Hz, with consistent high-magnitude coupling between the pressure and intensity oscillation after the in-phase forcing is turned on. This indicates stable, in-phase behavior between pressure and heat release characteristic of a linear and locked regime. Case B and C shows a broadening of the XWT magnitude in both time and frequency, showing signs of modulation and amplitude fluctuation. These suggest the onset of non-linear interactions between the flame and acoustics. At higher forcing amplitude the XWT magnitude becomes more intermittent, with localized bursts of strong coupling as

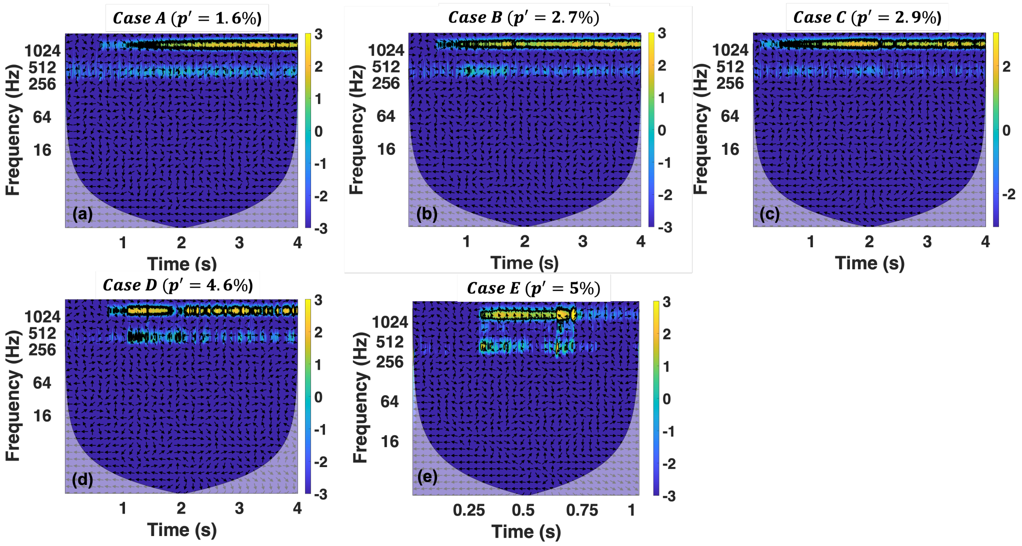

Figure 17: Cross-wavelet scalogram of the pressure and intensity fluctuations computed for Cases A-E clearly highlighting an intermittent variation in the amplitude of cross-wavelet transform between unsteady pressure and OH* intensity at high forcing amplitudes.

observed in Case D. This implies non-linear regime switching and temporal intermittency in flame response. The XWT magnitude increases during the wall-jet and wall-flame state, whereas it peaks up during the V-flame state. The coupling appears sporadic and weak in places for Case E, with energy dispersing across neighboring frequencies. This indicates loss of phase locking and potential flame–acoustic decoupling, consistent with near-blow-off behavior.

Thus, using XWT analysis it is obsevred that at low forcing amplitude, the system is stable and well-synchronized. As the forcing amplitude increases, the flame dynamics become increasingly non-linear, intermittent, and ultimately unstable—providing critical insight into the progression towards flame-blow-off.

3.3. Flame blow-off at higher amplitudes of excitation?

In this section, we discuss the process of flame blow-off at high amplitudes of acoustic excitation. It is observed that at high amplitudes of acoustic excitation (5% of mean atmospheric pressure - 0.91 bar) the flame blows-off. In this section, the flame blow-off mechanism during the high amplitude of acoustic forcing is discussed. It should be noted that the reason discussed here for flame blow-off is one of the many possible ways flame blow-off can occur. Figure 18a shows the time series of OH* intensity spatially-averaged over entire field-of-view. The dotted red line marks the instance when the acoustic excitation is turned on - $0.26s$. Figure 18b shows the time-averaged distribution of OH* intensity (top row), streamwise (u_x) (middle row) and radial (u_r) (bottom row) during the time events TA1 (first column), TA2 (second column) and TA3 (third column) marked in the figure 18a. The white contour represents $u_x = 0$ isoline. The vectors represent the total velocity vector. It is observed that post acoustic excitation, there is an increase in the mean OH* intensity (spatially averaged over entire field-of-view) (marked as time duration T1 in the figure 18a). This increase in the mean OH* is indicative of higher burning intensity possibly due to enhanced mixing of fuel/air mixture (due to strong velocity oscillations induced by transverse acoustic excitation) (observed through time-averaged OH* field for the unforced flame (duration TA1; first row and first column) than during the forced IP flame (duration - TA2; first row and second column) in figure 18b). Comparing the velocity field of the unforced and IP forced flame, it is observed that the annular jet and the central recirculation bubble in the forced IP flame becomes more compact (middle row: first and second column in figure 18b). After a certain duration of time, the flame blows-off and OH* intensity drops to zero (marked as T2). When the flame blows-off, it is observed through the time-averaged velocity field that the flowfield is in the wall-jet (WJ) state (third column in figure 18b).

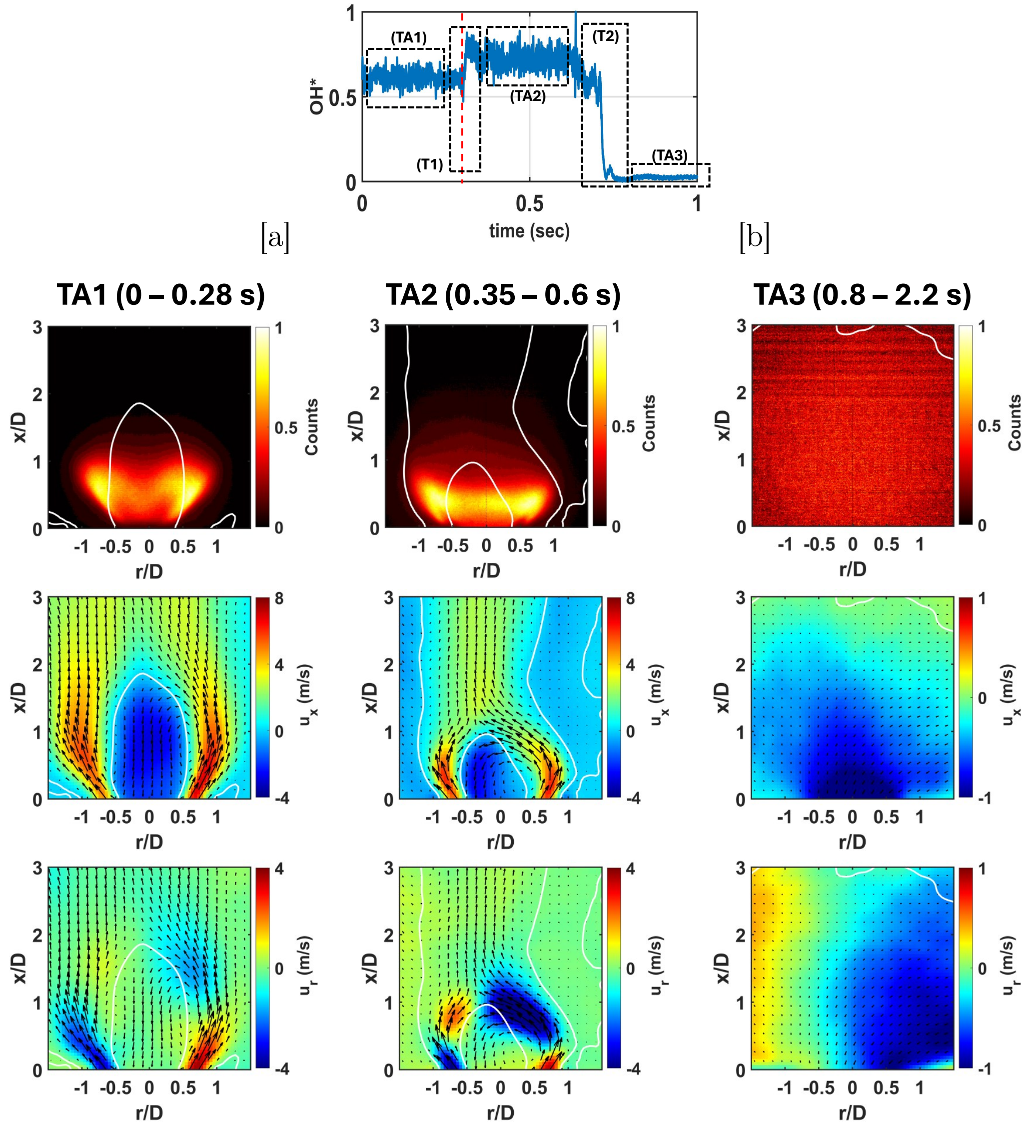

Figure 18: Case E: (a) Time series of OH* intensity spatially-averaged over entire field-of-view at different instants in time. The dotted red line marks the instance the acoustic excitation is turned on - 0.26 s. Five dotted black rectangles marked as TA1, T1, TA2, T2 and TA3 correspond to five different events; (b) time-averaged distribution of OH* intensity (top row), streamwise (u_x) (middle row) and radial (u_r) (bottom row) during the time events TA1 (first column), TA2 (second column) and TA3 (third column) marked in (a). The white contour represents $u_x = 0$ iso-curve. The vectors represent the total velocity vector.

Thus, it is observed in the present study with operating conditions ($Re = 3000$, $SN_G = 1.049$, $\phi = 1.0$), the flame extinguishes at high amplitudes ($> 5\%$) of acoustic excitations due to transition of the flow (and flame) to wall-jet state (WJ) where the flame stabilization is difficult to achieve. At $p' = 4.6\%$ the transition of the flame (and flow) from V-flame (or columnar-jet (CJ)) to wall-jet flame (or wall-jet flow (WJ)) was also observed where the flame showed repetitive oscillation between V-flame to wall-jet flame. Since the flame during the oscillation process did not stay for a long duration of time in the wall-jet state, the heat loss to the combustor dump plane may not have been sufficient for the flame to blow-off, although a number of extinction and re-ignition events are observed in the wall-jet state. Through these varying observations, we believe that the response of the flame is velocity-coupled i.e. the flame's response is dependent on the response of the flow field to the external transverse acoustics.

4. Conclusion

This study provides a detailed experimental investigation into the non-linear response of a swirl-stabilized, partially-premixed methane-air flame under large-amplitude in-phase transverse acoustic excitation. Utilizing high-fidelity diagnostics, including time-resolved 2D-2C PIV, OH* chemiluminescence, and unsteady pressure measurements, the work reveals how increasing acoustic forcing amplitude significantly alters flame topology, flow structure, and system dynamics. The injector features an axial swirler (geometric swirl number= 1.049), a centerbody acting as a fuel injector (with radial injection of fuel in the circumferential direction 12.5 mm upstream to the combustor dump plane), and a converging-diverging passage. The flow Reynolds number ($Re = 3000$), geometric swirl number ($SN_g = 1.049$), and global equivalence ratio ($\Phi = 1.0$) are kept constant during the investigation.

At low excitation amplitudes, the flame remains in a V-shaped configuration and responds linearly to the acoustic field. As the forcing amplitude increases beyond 2.7% of the mean chamber pressure, the system transitions into a non-linear regime marked by intermittent bursts of pressure oscillations, modulated flame structures, and quasi-periodic behavior. At 4.6%, a pronounced Type-II intermittency is observed where the flame cyclically transitions between V-shaped and wall-flame configurations. The velocity measurement of the flame indicates that the flow continuously oscillates between a columnar jet and a wall jet state (similar to the one observed in non-reacting swirl jet). Therefore, the mechanism behind the continuous change in flame topology is attributed to the change in the vortex breakdown states at these high amplitude acoustic oscillations. At 5%, the flame ultimately blows-out. Such a high-amplitude-acoustic induced blow-out is attributed to the transition of the swirling jet to a steady wall-jet state. We hypothesize that proximity of the flame to the combustor dump plane in the wall-jet state leads to a significant heat loss from the flame causing the blow-out. Through these varying observations (repetitive oscillation of the flame from V-flame to wall-jet flame, and flame blow-off at higher amplitudes of acoustic excitation due to the flow field transitioning to the wall-jet state), we believe that the response of the flame is velocity-coupled i.e. the flame's response is dependent on the response of the flow field to the external transverse acoustics. This study underscores the critical role of high-frequency thermo-acoustic oscillations in governing the stability and topology of swirl-stabilized flames. These oscillations, often encountered in modern gas turbine combustors—especially those employing hydrogen-rich fuels—can initiate strong velocity fluctuations and complex non-linear interactions between flow, heat release, and acoustics. The flame's response is shown to be velocity-coupled, with the flow's receptivity to transverse forcing determining the occurrence of dynamic flame transitions and extinction events.

The insights gained from this investigation are highly relevant for the design and control of advanced propulsion and power generation systems. They highlight the limitations of linear models and the necessity of incorporating non-linear dynamics and intermittency analysis to accurately predict and mitigate combustion instabilities under high-amplitude acoustic excitation.

CRediT authorship contribution statement

Ravi Gupta: Methodology, Investigation, Data curation, Visualization, Validation, Formal analysis, Writing – original draft. **Pratikash Panda:** Conceptualization, Methodology, Formal analysis, Writing - original draft, Writing - review & editing, Supervision, Project administration, Funding acquisition.

Declaration of competing interest

The authors declare that they have no known competing financial interests or personal relationships that could have appeared to influence the work reported in this paper.

Acknowledgement

The authors gratefully acknowledge financial support from the Department of Science and Technology (DST), India, through the Core Research Grant No. CRG/2020/004806, and the Ministry of Human Resource and Development (MHRD), India.

The authors thank project staff - Aayushi Bohrey and Shiv Prateek for their support while conducting the experiments.

The authors would also like to acknowledge the facilities provided by the DST–National Center for Combustion Research and Development (NCCRD) for conducting the experiments.

References

[1] T. C. Lieuwen, Unsteady combustor physics, Cambridge University Press, 2021.

[2] L. Rayleigh, The explanation of certain acoustical phenomena, Roy. Inst. Proc. 8 (1878) 536–542.

[3] T. Lieuwen, H. Torres, C. Johnson, B. Zinn, A mechanism of combustion instability in lean premixed gas turbine combustors, J. Eng. Gas Turb. Power 123 (2001) 182–189.

[4] S. Candel, Combustion dynamics and control: Progress and challenges, Proc. Combust. Inst. 29 (2002) 1–28.

[5] A. P. Dowling, Y. Mahmoudi, Combustion noise, Proc. Combust. Inst. 35 (2015) 65–100.

[6] T. C. Lieuwen, V. Yang, Combustion instabilities in gas turbine engines: operational experience, fundamental mechanisms, and modeling, American Institute of Aeronautics and Astronautics, 2005.

[7] F. Culick, P. Kuentzmann, Unsteady motions in combustion chambers for propulsion systems (2006).

[8] N. A. Worth, J. R. Dawson, Self-excited circumferential instabilities in a model annular gas turbine combustor: Global flame dynamics, Proc. Combust. Inst. 34 (2013) 3127–3134.

[9] A. Alhaffar, V. Latour, C. Patat, D. Durox, A. Renaud, J.-B. Blaisot, S. Candel, F. Baillot, Comparison of pressure-based flame describing functions measured in an annular combustor under self-sustained oscillations and in an externally modulated linear combustor, Proc. Combust. Inst. 40 (2024) 105249.

[10] A. Saurabh, C. O. Paschereit, Dynamics of premixed swirl flames under the influence of transverse acoustic fluctuations, Combust. Flame 182 (2017) 298–312.

[11] A. Saurabh, C. O. Paschereit, Premixed flame dynamics in response to two-dimensional acoustic forcing, Combust. Sci. Technol. (2018).

[12] T. Smith, B. Emerson, W. Proscia, T. Lieuwen, Role of induced axial acoustics in transverse acoustic flame response, Combust. Flame 195 (2018) 140–150.

[13] J. O'Connor, T. Lieuwen, Disturbance field characteristics of a transversely excited burner, Combust. Sci. Technol. 183 (2011) 427–443.

[14] J. O'Connor, T. Lieuwen, Recirculation zone dynamics of a transversely excited swirl flow and flame, Phys. Fluids 24 (2012) 2893–2900.

[15] J. O'Connor, N. A. Worth, J. R. Dawson, Flame and flow dynamics of a self-excited, standing wave circumferential instability in a model annular gas turbine combustor, Vol. 55119, Turbo Expo: Power for Land, Sea, and Air, American Society of Mechanical Engineers, 2013.

[16] F. Lespinasse, F. Baillot, T. Boushaki, Responses of v-flames placed in an hf transverse acoustic field from a velocity to pressure antinode, CR Mecanique 341 (2013) 110–120.

[17] D. Brouzet, S. You, M. A. Plascencia, M. Roa, M. Ihme, The dynamics of non-premixed flames subjected to a transverse acoustic mode, Combust. Flame 246 (2022) 112330.

[18] M. Hauser, M. Lorenz, T. Sattelmayer, Influence of transversal acoustic excitation of the burner approach flow on the flame structure, Vol. 43970, Turbo Expo: Power for Land, Sea, and Air, 2010.

[19] M. Malanoski, M. Aguilar, V. Acharya, T. Lieuwen, Dynamics of a transversely excited swirling, lifted flame: Part I— Experiments and data analysis, Vol. 1B: Combustion, Fuels and Emissions, ASME Turbo Expo 2013: Turbine Technical Conference and Exposition, American Society of Mechanical Engineers, 2013.

[20] M. Fleifil, A. M. Annaswamy, Z. Ghoneim, A. F. Ghoniem, Response of a laminar premixed flame to flow oscillations: A kinematic model and thermoacoustic instability results, Combust. Flame 106 (1996) 487–510.

[21] A. Renaud, T. Yokomori, S. Tachibana, Study of a thermo-acoustic instability triggering in a low-swirl burner using simultaneous time-resolved acetone and oh-plif, Proc. Combust. Inst. 37 (2019) 2627–2633.

[22] A. Peracchio, W. Proscia, Nonlinear heat-release/acoustic model for thermoacoustic instability in lean premixed combustors, Vol. 78644, Turbo Expo: Power for Land, Sea, and Air, American Society of Mechanical Engineers, 1998.

[23] T. Lieuwen, Theoretical investigation of unsteady flow interactions with a premixed planar flame, J. Fluid Mech. 435 (2001) 289–303.

[24] T. Poinsot, D. Veynante, F. Bourienne, S. Candel, E. Esposito, J. Surget, Initiation and suppression of combustion instabilities by active control, Symp. (Int.) Combust. 22 (1989) 1363–1370.

[25] A. P. Dowling, Nonlinear self-excited oscillations of a ducted flame, J. Fluid Mech. 346 (1997) 271–290.

[26] L. Kabiraj, R. I. Sujith, Nonlinear self-excited thermoacoustic oscillations: intermittency and flame blowout, J. Fluid Mech. 713 (2012) 376–397.

[27] B. Mohan, S. Mariappan, Self-excited intermittent thermoacoustic fluctuations in an annular combustor exhibiting flame transient phenomena: Physical mechanisms and modeling, Phys. Fluids 35 (2023) 045134.

[28] D. Durox, K. Prieur, T. Schuller, S. Candel, Different flame patterns linked with swirling injector interactions in an annular combustor, J. Eng. Gas Turb. Power 138 (2016) 101504.

[29] P. Auzillon, D. Durox, T. Schuller, J. Moeck, Swirling spray flames dynamical blow-out induced by transverse acoustic oscillations, Combust. Flame 245 (2022) 112357.

[30] T. Lee, K. T. Kim, High-frequency transverse combustion instabilities of lean-premixed multislit hydrogen-air flames, Combust. Flame 238 (2022) 111899.

[31] B. Ahn, T. Indlekofer, J. R. Dawson, N. A. Worth, Heat release rate response of azimuthal thermoacoustic instabilities in a pressurized annular combustor with methane/hydrogen flames, Combust. Flame 244 (2022) 112274.

[32] H. Paniez, S. Marragou, H. Magnes, T. Schuller, High-frequency thermoacoustic instability in a dual swirl h2 burner, Proc. Combust. Inst. 40 (2024) 105679.

[33] A. K. Gupta, D. G. Lilley, N. Syred, Swirl flows, Tunbridge Wells (1984).

[34] B. Wieneke, Piv uncertainty quantification from correlation statistics, Meas. Sci. Technol. 26 (2015) 074002.

[35] A. Sciacchitano, B. Wieneke, Piv uncertainty propagation, Meas. Sci. Technol. 27 (2016) 084006.

[36] K. Klimaszewska, J. J. Żebrowski, Detection of the type of intermittency using characteristic patterns in recurrence plots, Phy. Rev. E 80 (2009) 026214.

[37] Y. Pomeau, P. Manneville, Intermittent transition to turbulence in dissipative dynamical systems, Comm. Math. Physics 74 (1980) 189–197.

[38] R. Gupta, R. Gohiya, P. Panda, Columnar-jet to wall-jet state transition in transversely excited swirling flow, Phys. Fluids 35 (2023).

Appendix A. Instantaneous OH* and velocity field during the extinction event

This section discusses the instantaneous time snapshots for Case E during the transient events (T1 and T2) marked in the figure 18a. The transition of the flame and flow from unforced state to a more compact (in the streamwise direction) and wider flame is observed through instantaneous OH* intensity and streamwise velocity (u_x) shown in the figure A.19a (time duration marked as T1 in the figure 18a). Similarly, through the instantaneous OH* and streamwise velocity (u_x) as shown in figure A.19b, it is observed that during the extinction phase (marked as $T2$ in the figure 18a), the compact and wide flame transitions to a wall-jet flame. The flame in the wall-jet state sits on the dump plane, and due to its close proximity to the dump plane, there is a heat loss to the dump plane. This heat loss to the dump plane results in the flame blow-off. The range of OH* intensity distribution in figure A.19b is kept variable to allow ease of visualization of blow-off sequence. Thus, it is observed that at higher amplitudes of acoustic excitation, the flame blows-off due to the V-flame transitioning into the wall-jet flame (in parallel, the flow field transitions from columnar-jet (CJ) to wall-jet (WJ)), and the wall-jet flame is unable to sustain due to heat loss to the combustor dump plane.

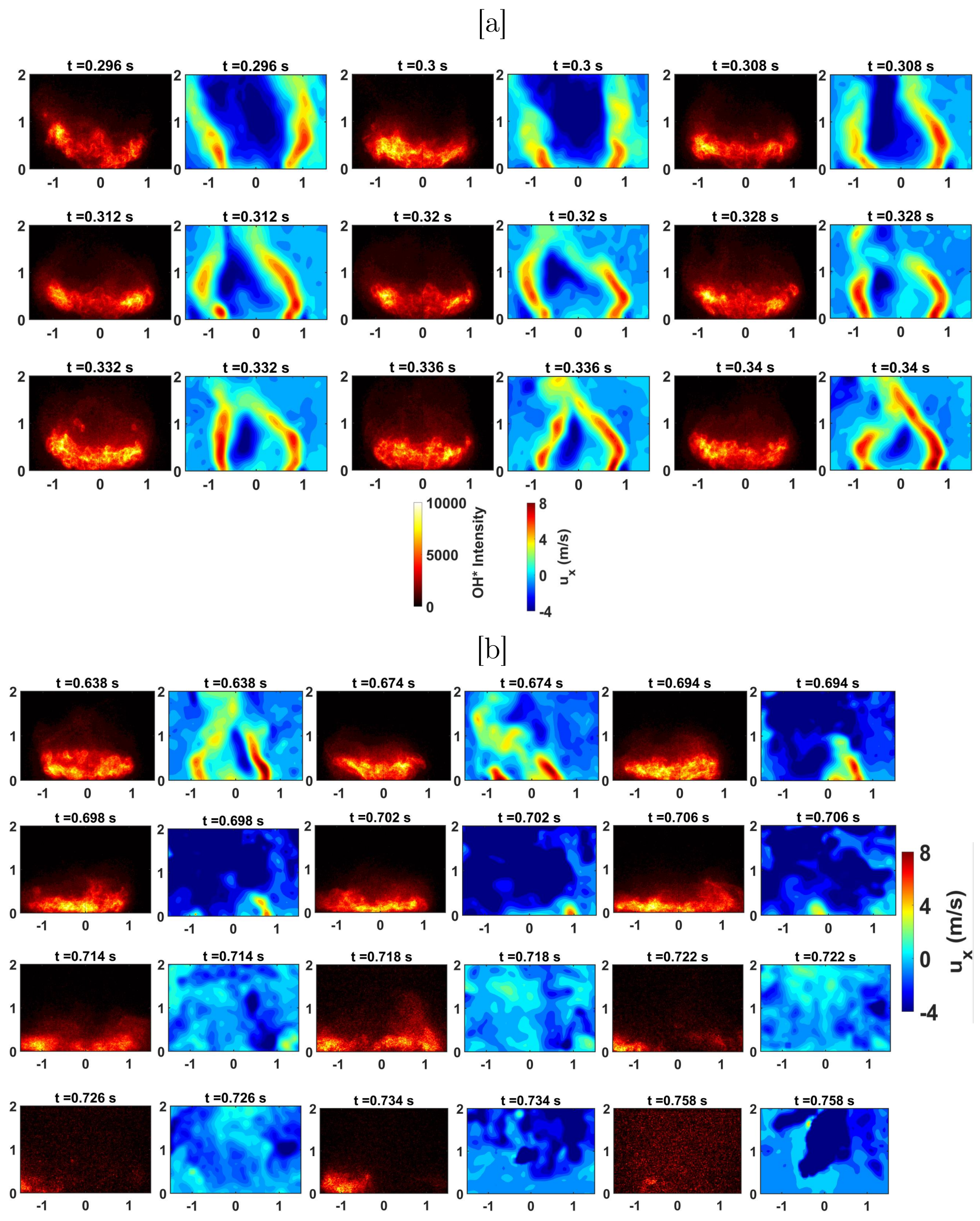

Figure A.19: Case E: Instantaneous OH* intensity and streamwise velocity (u_x) at different instants in time marked as (a) T1, and (b) T2, in the figure 18a. The range of OH* intensity distribution in (b) is kept variable to allow ease of visualization of blow-off sequence.